

Modeling Mid-Ultraviolet Spectra. I. Temperatures of Metal-Poor Stars^{1,2}

Ruth C. Peterson³, Ben Dorman⁴, and Robert T. Rood⁵

ABSTRACT

Determining the properties of remote globular clusters and elliptical galaxies using evolutionary population synthesis requires a library of reliable model stellar fluxes. Empirical libraries are limited to spectra of stars in the solar neighborhood, with nearly solar abundances and abundance ratios. We report here a first step towards providing a flux library that includes nonsolar abundances, based on calculations from first principles that are calibrated empirically. Because the mid-ultraviolet spectrum of an old stellar system is dominated by the contribution from its main-sequence turnoff stars, we have started by modeling these. We have calculated mid-ultraviolet spectra for the Sun and nine nearby, near-main-sequence stars spanning metallicities from less than 1/100 solar to greater than solar, encompassing a range of light-element abundance enhancements.

We first determined temperatures of eight of the stars by analyzing optical echelle spectra together with the mid-ultraviolet. Both could be matched at the same time only when models with no convective overshoot were adopted, and only when an approximate chromosphere was incorporated near the surface of relatively metal-rich models. Extensive modifications to mid-UV line parameters were also required, notably the manual assignment of approximate identifications for mid-UV lines missing from laboratory linelists. Without recourse to additional missing opacity, these measures suffice to reproduce in detail almost the entire mid-UV spectrum of solar-temperature stars up to one-tenth solar metallicity, and the region from 2900 Å to 3100 Å throughout the entire metallicity range. Ramifications for abundance determinations in individual metal-poor stars and for age-metallicity determinations of old stellar systems are briefly discussed, with emphasis on the predictive power of the calculations.

¹Based on observations obtained with the Hubble Space Telescope of Space Telescope Science Institute, under contract with the National Aeronautics and Space Administration (NASA).

²Based on observations obtained with the Shane Telescope at Mt. Hamilton, UCO/Lick Observatory.

³UCO/Lick Observatory, Dept. of Astronomy, University of California, Santa Cruz, CA 95064, and Astrophysical Advances, Palo Alto, CA 94301; peterson@ucolick.org.

⁴Emergent-IT Inc. and Goddard Space Flight Center, Greenbelt, MD 20771; Ben.Dorman@gssc.nasa.gov.

⁵Dept. of Astronomy, University of Virginia, P.O. Box 3818, Charlottesville, VA 22903-0818; rtr@veris.astro.virginia.edu.

Subject headings: stars: abundances — stars: fundamental parameters — stars: Population II — galaxies: abundances — ultraviolet: galaxies — ultraviolet: stars

1. Introduction

To characterize the metallicity and age of an old stellar system, iron abundance $[\text{Fe}/\text{H}]$ (the logarithm of the iron-to-hydrogen abundance ratio with respect to its solar value) and the stellar effective temperature T_{eff} must be determined together for its main-sequence turnoff (MSTO) stars. These are dwarfs and subgiants of types F and early G with $5750 \leq T_{\text{eff}} \leq 7000$ K. Their spectra are dominated by Fe I lines, whose strength increases as T_{eff} declines. For both metallicity and age, then, a reliable derivation of T_{eff} is necessary.

This can be problematical even for an individual star. The photometric colors often used to derive T_{eff} are sensitive to reddening by the interstellar medium and to the modeling of convection (Castelli, Gratton, & Kurucz 1997), as is the more recently developed infrared flux method (Alonso, Arribas, & Martinez-Roger 1996). Methods using Balmer-line profiles are reddening-independent but still very model-dependent (Magain 1984; Fuhrmann, Axer, & Gehren 1994). Methods relying on the excitation equilibrium of Fe I are reddening-independent and model-independent if lines are weak, but are susceptible to systematic errors in laboratory measurements of gf-values (Blackwell et al. 1982) and to possible departures from local thermodynamic equilibrium (LTE; Thévenin & Idiart 1999).

Currently, T_{eff} values derived for individual MSTO stars show uncomfortably large spreads: values of Carney et al. (1994) and Fulbright (2000) average 100 K – 200 K lower than those found by King (1993) and Gratton, Carretta, & Castelli (1996), with those of Alonso, Arribas, & Martinez-Roger (1996) and Blackwell & Lynas-Gray (1998) in between. Not only is overall metallicity affected, but also the ratios of the abundance with respect to iron of certain elements. Among these are the $[\text{Li}/\text{Fe}]$ and $[\text{O}/\text{Fe}]$ ratios so critical to uncovering the nucleosynthesis history of the early universe (Spite et al. 1996) and deducing the age of globular clusters from the MSTO luminosity (VandenBerg & Bell 2000). When T_{eff} alone is raised by 100 K, modeled values of $[\text{Li}/\text{Fe}]$ change by +0.09 dex (Spite et al. 1996); $[\text{O}/\text{Fe}]$ changes by –0.09 dex, +0.03 dex, or +0.16 dex depending on whether the high-excitation O I 7775 Å triplet, the [O I] 6300 Å ground-state line, or OH molecular lines near 3100 Å are used (Kraft 2000). Not surprisingly, the oxygen abundance in extremely metal-poor stars remains uncertain, as summarized during a workshop devoted to the problem (Kraft 2000; Balachandran 2000; Peterson 2000; Lambert 2000). King (1993) and Kraft (2000), among others, have suggested that a higher T_{eff} scale for metal-poor turnoff stars might eliminate the systematic differences in $[\text{O}/\text{Fe}]$ seen from its different diagnostics.

For all these reasons, it seems important to reduce uncertainties in the determination of T_{eff} in MSTO stars. Fitting the slope of their UV flux distribution might help, since the fluxes of F–G stars peak in the optical so that UV fluxes vary rapidly with T_{eff} . Although fitting a UV slope is also reddening-dependent, reddening should be very low for the brightest metal-poor MSTO stars, which are typically within 50 pc (e.g., Reid 1998).

Reliable calculations of MSTO mid-UV spectra would be especially valuable in constraining the age and metallicity of a spatially unresolved old stellar system such as an elliptical galaxy or

extragalactic globular cluster. For the mid-UV flux of an old stellar population is dominated by turnoff stars (Dorman, Rood, & O’Connell 1993), but the light redward of 4500 Å is dominated by cool giants in a 17 Gyr population of solar metallicity (Worthey 1994). To date, however, mid-UV studies of galaxies and globulars (e.g., Spinrad et al. 1997; Ponder et al. 1998) have largely been empirical, comparing extragalactic spectra against observed spectra of individual F and G stars (Fanelli et al. 1990). Thus the metallicity of the extragalactic systems has generally been assumed to be solar, although age is very sensitive to this assumption (Heap et al. 1998). Furthermore, nonsolar abundance ratios have not been included, despite the fact that abundance enhancements of light elements such as magnesium are generally seen in metal-rich extragalactic systems (Peterson 1976; O’Connell 1976; Worthey, Faber, & Gonzalez 1992; Henry & Worthey 1999).

Modeling the mid-UV region is difficult, though, because of the dramatic increase in line absorption at short wavelengths. Line blending in the solar spectrum suppresses the optical continuum blueward of ~ 4500 Å (Kurucz et al. 1984), and becomes even more severe in the near- and mid-UV. Especially in the UV, many lines are “missing” – although they appear as absorption features in spectra of solar-type stars, they lack laboratory identification, and are thus not matched by spectral synthesis calculations (Kurucz & Avrett 1981). As a result, the normalization of the solar UV continuum is controversial (Balachandran & Bell 1998; Boesgaard et al. 1999; Israelian et al. 2001).

With few exceptions (e.g., Heap et al. 1998), calculations of the mid-UV region are based on Kurucz model flux distributions. Allende Prieto & Lambert (2000) compared these to International Ultraviolet Explorer (IUE) mid-UV spectra of nearby metal-poor halo stars, illustrating that T_{eff} is generally recovered when parallaxes are known and reddening negligible. Lotz, Ferguson, & Bohlin (2000) have used Kurucz fluxes as generated by Lejeune, Cuisinier, & Buser (1997) to examine the effect of abundance on the mid-UV light of old stellar populations, but found that the UV fluxes of cool stars were poorly reproduced.

This is not surprising given the known limitations of the opacity distribution functions on which the Kurucz flux distributions are based. They statistically treat lines in a list that includes “predicted” lines whose wavelengths are uncertain by ~ 10 Å (because one or both energy levels have not been measured in the laboratory), limiting the resolution of the flux distributions to 10 Å. Moreover, they assume a solar iron abundance ~ 0.15 dex higher than the value currently accepted (Biémont et al. 1991; Holweger, Kock, & Bard 1995), and a solar ratio of light-element abundances $[\alpha/\text{Fe}] = 0$. In contrast, metal-poor stars of the Galactic halo typically show $[\alpha/\text{Fe}] = 0.3$ (Wheeler, Sneden, & Truran 1989), a factor-of-two enhancement in Mg, Si, Ca, and Ti. This affects the fit in the mid-UV, since it includes the very strong resonance doublet of Mg II at 2800 Å and a bound-free opacity edge of Mg I at 2512 Å, plus many weaker Mg, Si, and Ti lines.

2. Overview of This Work

In this work we calculate the mid-UV spectrum line-by-line at high resolution, independent of the Kurucz flux distributions. Our line list does not include predicted lines, but rather is based on an updated laboratory line list augmented by manual addition of missing lines where necessary. To ensure the reliability of these calculations, we match as best we can the individual line blends observed in the mid-UV echelle spectra of real near-turnoff stars, spanning a wide metallicity range and including both solar and enhanced light-element ratios. Our purpose is to reproduce mid-UV spectra of turnoff stars accurately enough to determine T_{eff} and to predict the composite mid-UV spectra of old stellar systems over their entire range of overall metallicity and light-element abundance ratio.

In this first step, we describe this calibration procedure. Because the calibrations depend significantly on the stellar temperatures adopted, we have carried out new T_{eff} determinations in seven metal-poor turnoff stars and one mildly metal-poor hotter star. They are based on simultaneously matching both mid-UV spectra (2280 – 3120 Å) and the H α profile and the strengths of high-excitation atomic lines in optical spectra. We thus do not rely on any photometry or parallax information in the T_{eff} determination. Iron abundances and $[\alpha/\text{Fe}]$ ratios were adopted as derived from both weak and strong lines in the optical spectra. To assist in filling in the mid-UV line list, we have included mid-UV analyses of two stars with mid-UV spectra of very high resolution, the Sun and HD 128620 (= α Cen A), a well-studied nearby southern star with a greater-than-solar metallicity (Neuforge-Verheecke & Magain 1997), for which T_{eff} was taken from the literature.

In fitting each mid-UV spectrum, we adopted a single continuum normalization constant, the scale factor by which the observed mid-UV spectral flux was multiplied to match the flux predicted by theoretical calculation. This constant proved to agree to an average of $6\% \pm 5\%$ with that expected from the ratio of stellar distance (found from the parallax) to stellar radius (found from the model $\log g$ assuming a reasonable stellar mass). Model $U - B$, $B - V$, and $b - y$ colors all agreed extremely well with those observed, confirming T_{eff} errors of $\lesssim 50$ K.

Our mid-UV and optical echelle spectra are described in §3. As discussed in §4, T_{eff} was initially established from the optical spectra, and compared to the mid-UV fit. For the most metal-poor stars, this fit did not require the addition of missing lines, but did require the use of Kurucz models in which convective overshoot was turned off, in contrast to the Kurucz models in general use. To reproduce mid-UV line strengths and to match the pseudocontinuum of the mid-UV spectra of more metal-rich stars, mid-UV atomic line parameters were changed and missing lines were added. Transitions especially sensitive to the surface temperature were still poorly reproduced; this mismatch was reduced by adopting a mild enhancement of temperatures in shallow photospheric layers of the models of one-tenth solar metallicity and higher.

The degree to which the resulting calculations match both mid-UV and optical spectra of turnoff stars is shown and discussed in §5. The match is very good for 2900 – 3120 Å at all metallicities, and generally good throughout the mid-UV for metallicities at and below one-third

solar. It could be improved at solar metallicities by obtaining additional high-resolution mid-UV spectra of a few well-chosen standards.

Our T_{eff} results are presented in §6, where comparisons are made of model fluxes and colors with observations. We conclude in §7 with a summary and a discussion of the prospects for constraining age and metallicity of quiescent stellar systems by comparing such calculations to spectra of their integrated light.

3. Observations

We begin by listing the properties of the stars considered in Table 1. The first five columns following the HD number give the observed V magnitude, colors, and the parallax from SIMBAD. The next five columns, discussed in §6, show comparisons of observed properties of each star with those calculated from the models. The parameters of the model used to calculate both mid-UV and optical spectra of each star are given in the next four columns. In all cases but HD 128620 = α Cen A and the Sun, all the model parameters were redetermined here as described below. The final columns show T_{eff} values determined previously in several works.

Of the eight stars whose temperatures have been redetermined here from optical and UV spectra, seven are metal-poor main-sequence turnoff (MSTO) stars. The eighth, HD 128167, is a mildly-metal poor star lying above the halo main-sequence turnoff, either younger or a blue straggler. It was included to give temperature leverage to the mid-UV comparisons, as discussed below. Likewise the Sun and α Cen A were included to represent the high-metallicity end. The solar parameters were considered so well determined that no re-evaluation was necessary. The star α Cen A was not reanalyzed because no optical spectrum was available: it is inaccessible from the northern hemisphere. Its T_{eff} and abundance have been determined to moderate accuracy from extensive abundance analyses, and its gravity as $\log g = 4.33 \pm 0.02$ as found from its visual and radial-velocity motion about its companion (Chmielewski et al. 1992; Neuforge-Verheecke & Magain 1997; Pourbaix et al. 1999). The iron abundance listed in Table 1 was adopted to best match its mid-UV spectrum.

Optical spectra were obtained for all stars in Table 1 but the Sun and α Cen A. The Lick Observatory Shane 3m echelle spectrograph (Vogt 1987) was used with a TEK 2048 \times 2048 CCD, at a FWHM resolution of 38,000. The spectra of HD 84937, HD 94028, and HD 106516 were kindly provided by Fulbright (2000). Exposure times on the 3m were typically 10min for all stars except HD 128167 (40s). Complete spectral coverage over 3900 Å – 7800 Å and S/N > 100/pixel were obtained in all cases but one, although fringing compromises the accuracy of the data at the long-wavelength end of the range. For the one exception, HD 114762, the blue spectrum was obtained in two one-hour exposures by Tony Misch at Lick with the coude auxiliary telescope, using the same echelle spectrograph configuration. For the Sun, the flux spectrum of Kurucz et al. (1984) was downloaded from the Kurucz web site at <http://cfaku5.harvard.edu>; the full-resolution version

was matched at 150,000 resolution.

The mid-UV spectral observations of the Sun modeled here are the rocket spectra of Kurucz & Avrett (1981), recorded on film. Both passes of the center of the solar disk were used. Gaussian broadenings of 1.5 km s^{-1} for macroturbulence and 80,000 FWHM for other broadening sources provided a good match. A constant normalization scale factor of 1.10 was adopted, in keeping with the stated 10% uncertainty of its flux calibration.

The stellar UV spectra were obtained with the Space Telescope Imaging Spectrograph (STIS) of Hubble Space Telescope (HST) from mid-1998 to mid-1999. Salient features are noted here; full details may be found from the HST archive at <http://archive.stsci.edu>.

To obtain the mid-UV spectra of most stars, the near-UV MAMA detector was used with the STIS E230M grating over its default range of $2280 \text{ \AA} - 3120 \text{ \AA}$ at a FWHM resolution $\sim 25,000$. HD 106516 (= HR 4657) was observed by Heap et al. (1998) in program #7433 with the 0.2×0.06 aperture. Mid-UV spectra for HD 19445, HD 84937, HD 94028, HD 114762, HD 184499, and HD 201891 were acquired in snapshot program #7402 by Peterson & Schrijver (2000), with two exposures obtained for HD 19445, HD 84937, and HD 114762. The 0.2×0.2 aperture was used and exposure times were 6 – 10 min. Consequently, S/N is lower, but flux levels are less dependent on pointing. Fluxes good to 1% for these six stars are indicated by previous observations of Mg II line profiles in each star, made using the HST Goddard High-Resolution Spectrograph (GHRS) and the 2×2 aperture in program #5869 (Peterson & Schrijver 1997).

Mid-UV spectra of the stars HD 128167 (=HR 5447), from #7433, and HD 128620 (= HR 5459 = α Cen A), from #7263 (Linsky et al. 2000), were recorded in multiple exposures with the E230H grating. Spectral coverage is $2380 \text{ \AA} - 3160 \text{ \AA}$ for HD 128167 and $<2280 \text{ \AA} - 3160 \text{ \AA}$ for HD 128620. A FWHM resolution of $\sim 60,000$ was achieved with the 0.2×0.06 aperture for HD 128167, and the $0.2 \times 0.05\text{ND}$ aperture for HD 128620. For neither star do fluxes always reproduce exactly in orders obtained in more than one exposure; differences as large as 10% are seen. Similar uncertainties are anticipated for HD 106516, where the 0.2×0.06 aperture was also used.

Rotation is detected in at least two stars and possibly in two more, from the extra broadening required to match line profiles. For HD 128167, HD 106516, HD 84937, and HD 114762, line breadths were matched in the spectral synthesis by adopting rotational velocities $v \sin i = 9, 7, 5,$ and 4 km s^{-1} respectively. Thus the resolution of the mid-UV spectrum of HD 128167 is effectively degraded to that of the stars observed at lower resolution, affecting the discernment of mid-UV lines. This star nonetheless has one of the sharpest-lined spectra among those obtained in program #7433.

4. Spectrum Analysis

Spectrum analysis was based on visually matching each observed spectrum to *ab initio* radiative-transfer calculations assuming static models in LTE. The program SYNTHE (Kurucz & Avrett

1981), the Kurucz (1995) and Castelli et al. (1997) grids of ATLAS9 models, and the Kurucz line lists for atomic species and molecular hydrides were downloaded from the Kurucz web site, where further details on each of these can be found. As described below, all models, including that of the Sun, were ultimately drawn from the Castelli et al. (1997) grid alone. The more metal-rich ones were modified by introducing enhanced temperatures in the shallow layers.

The SYNTHE program accepts as input both line lists and a model atmosphere with temperature and other quantities tabulated for each depth, and calculates an array of spectra at individual emergent angles. These may then be used individually (as for spectra of the center of the solar disk) or convolved with a zero or positive rotational velocity to generate an emergent flux spectrum. In either case, the resulting spectrum can be broadened by Gaussians (or other profile shapes) to incorporate macroturbulence and instrumental broadening.

SYNTHE was modified to run under UNIX on a Sun Ultra-30 at the University of Virginia. Mid-UV spectra from 2280 Å to 3160 Å were calculated at a resolution of 330,000 (500,000 for the Sun and HD 128620), and optical spectra at a resolution of 500,000. A Gaussian macroturbulent broadening of 1.5 km s^{-1} was assumed for all stars as well as for the Sun. Spectra for some stars were rotationally broadened as listed in the last paragraph of §3, as was the solar flux spectrum, for which a mean rotational velocity of 2 km s^{-1} was adopted. The spectra were then broadened by Gaussians corresponding to the values of instrumental resolution listed individually in §3.

The line lists and the source code of the opacity routines available at the Kurucz web site give specifics on the wide variety of opacity sources treated by SYNTHE. For example, the significant absorption by the bound-free absorption edge of Mg I near 2512 Å is treated both as line opacity, with the line list including the bound-bound transitions to $N \sim 60$, and as continuous opacity blueward of the bound-free edge at $\nu_o = 39759.8 \text{ cm}^{-2}$, by the subroutine MG1OP. Near ν_o , this routine adopts a cross section of 40 Mbarn with a $(\nu/\nu_o)^{-14}$ frequency dependence, based on the laboratory measurement of $46 \pm 12 \text{ Mbarn}$ by Lombardi, Smith, & Parkinson (1981) and the convergence of high-level lines. Where this formalism falls below the theoretical cross section, the program adopts the latter, with a cross section of 20 Mbarn and a $(\nu/\nu_o)^{-2.7}$ frequency dependence (e.g., Butler et al. 1993).

For calculations redward of 5000 Å, the line list of Peterson, Dalle Ore, & Kurucz (1993) based on the solar spectrum was adopted, with modifications due to the use here of a flux, rather than central intensity, spectrum for the Sun and to the incorporation of an approximate chromosphere in the solar model. This led to the deduction of larger gf-values for the strongest lines except where laboratory gf-values were adopted, as for low-excitation Fe I lines with furnace measurements (Blackwell et al. 1982).

Blueward of 5000 Å, the Kurucz 25 May 1998 atomic line lists *gf0300.100*, *gf0400.100*, and *gf00500.100* were used. These differ significantly from those used in the Kurucz flux distribution calculations in including only atomic lines identified in the laboratory (with laboratory gf-values where available) – like those of Kurucz & Bell (1995) but with the addition of many lines of Fe I, Fe II,

and other species whose upper energy levels were newly determined in near-UV laboratory spectra (e.g., Nave et al. 1994). Because the strengths or profiles of many lines were mismatched when using line parameters directly from this list, their gf-values and damping constants were changed where necessary, as described shortly. Since many lines appear in the STIS mid-UV spectra that were not modeled by lines in the list, such missing lines were added blueward of 3120 Å. Redward of this, no missing lines were added, but gf-values were changed to match stronger lines in the Sun in the regions depicted in Fig. 4 below.

The T_{eff} , $\log g$, $[\text{Fe}/\text{H}]$, χ_t , and $[\alpha/\text{Fe}]$ values for each reanalyzed star were initially established from H α and weak lines of neutral species in the optical spectra, reassessed from optical lines of once-ionized species, then confirmed or revised from the UV. For the two most metal-poor stars, mid-UV spectra provided an immediate check on T_{eff} . For the others, the following steps were iterated until all diagnostics converged.

First the H α profile and an assumed $\log g$ were used to estimate T_{eff} . $[\text{Fe}/\text{H}]$ was adjusted until weak Fe I lines in the 5100 Å – 5400 Å region were well matched; their strengths are largely gravity-independent. The strength of weak Ti I, Mg I, and Si I lines determined $[\alpha/\text{Fe}]$. Microturbulent velocity χ_t was set by matching weak and strong iron and titanium lines. Gravity $\log g$ was then checked by demanding matches for Mg I, Mg II, and the wings of the Mgb lines, for Fe I and Fe II, for Ti I and Ti II, and for Si I and Si II. This also constrains T_{eff} , for the Mg II and Si II doublets arise from highly excited lower levels (>8 eV), while the optical Ti II and Fe II lines originate from much lower levels (<3 eV). Roughly two dozen Fe I lines, a dozen Ti I lines, and a dozen total Ti II and Fe II lines were detected for the most metal-poor stars, with double this number typical of the more metal-rich stars. The Mg II and Si II doublets at 4481 Å and at 6347.1 and 6371.3 Å were seen in all cases, but Si II only marginally so in HD 84937 and HD 19445.

Once the diagnostics began to converge, iterative adjustments were made to the Kurucz mid-UV atomic-line parameters. First, gf-values were modified for atomic lines identified in the laboratory. The relative contribution of identified lines to a blend was ascertained from the behavior of the blend in the hot star HD 128167 versus the cooler ones, and in the higher-gravity stars such as HD 19445 versus the lower-gravity ones. Damping constants were changed in some cases to match line profiles. Damping constants rather than gf-values were changed for the strong resonance lines well-observed in the interstellar medium for which gf-values are tabulated by Morton (1991).

Next, for lines lacking identification, the laboratory line list was searched for transitions close enough in wavelength to perhaps be responsible. The gf-value of a nearby identified line was increased by up to 4.5 in the log, and the calculation repeated. This line was dropped if still not strong enough; otherwise its gf-value was adjusted to match. The high resolution of the α Cen A and solar spectra showed that most such identifications were very well matched in wavelength, and thus likely to be correct, when based on increases of ≤ 2.5 in the log.

For the two most metal-poor stars, these steps were sufficient to enable the continuum to be defined unambiguously throughout most of the mid-UV region. Its definition in more metal-

rich stars was hampered by line crowding, yielding a pseudocontinuum that the modeling did not properly reproduce.

Much of this pseudocontinuum mismatch appeared to be due to individual transitions missing from the line list. This was indicated by the very common occurrence throughout the mid-UV of unmodeled absorption features found at the same wavelengths in all stars, features whose strength steadily increased in going from weak-lined to strong-lined spectra. Most of these transitions are weak, consistent with the fact that the intrinsically strongest transitions of each species are the ones most likely to have been detected in the laboratory.

Except just redward of the Mg I edge at 2512 Å, most missing lines are probably due to iron. Its abundance is high and the spectra are rich in lines of Fe I and Fe II, which are well-populated species in solar-temperature stars. Of the elements with similar first ionization potentials, only magnesium and silicon have comparable abundances; the mid-UV spectra of their low-ionization stages are generally much less complex, as are those of the more abundant CNO elements. While iron-peak elements such as Cr, Mn, and Ni have many transitions throughout the mid-UV, iron dominates because it is twenty or more times as abundant. In most halo stars above one-tenth solar metallicity, the relative abundances of these elements with respect to iron are within 0.2 dex of those of the Sun (although larger differences may occur, especially at very low metallicity: McWilliam et al. 1995; Nissen et al. 2000; Prochaska & McWilliam 2000). The mismatch that will result from assigning missing lines of these elements to iron should be mild.

In the region immediately redward of the bound-free Mg I opacity edge at 2512 Å, the probability is significant that missing lines may be due to magnesium rather than iron. Redward of the edge there are a very large number of transitions to known highly excited levels of the Mg I atom, and presumably a very large number of similar transitions to closely-spaced highly excited levels that are as yet unidentified in the laboratory. If many weak transitions redward of 2512 Å are due to magnesium but have been assigned to iron instead, our calculations will underestimate the absorption in this region in metal-rich alpha-enhanced populations. We see below that this region is poorly modeled in any case once metallicity exceeds one-tenth solar.

The modeling then proceeded iteratively by assigning tentative identifications and transition probabilities to each missing feature, then recalculating until an acceptable match was achieved or deemed unattainable with existing data (as for the regions just redward of 2550 Å and 2640 Å in the solar spectrum). Features were attributed to either low-excitation Fe I, moderate-excitation Fe I, or Fe II, whose line strengths depend differently on stellar temperature and gravity (pressure) because of the Boltzmann and Saha equations. With a $T_{\text{eff}} \sim 1000$ K higher than those of other moderately weak-lined stars, HD 128167 proved exceptionally useful in making these assignments. The higher resolution of the spectra of the strong-lined stars HD 128620 = α Cen A and the Sun was essential in discerning the wavelengths of the many features emerging above one-third solar metallicity.

A brief examination was made of the gf-value changes for low-excitation Fe I lines, namely those identified in the laboratory with (air) wavelengths falling between 2600 Å and 3000 Å, and

with a lower level of $6000 - 10000 \text{ cm}^{-1}$ and an upper level of $40000 - 50000 \text{ cm}^{-1}$. Sixty-five such Fe I lines have gf-values from the laboratory measurements of O’Brian et al. (1991); 52 were not changed, while 13 were changed by from -0.6 to $+0.4$ dex. Nine lines have gf-values from the laboratory measurements of Fuhr, Martin, & Wiese (1988); five were unchanged, and four changed by from -0.7 to -0.3 dex. Thus the mid-UV gf-values found in this work generally concur with the mid-UV laboratory measurements.

In contrast, fifteen lines have theoretical gf-values from Kurucz (1994); four were not changed, but 11 were changed by from -2.2 to $+0.6$ dex, all but one decreased. The theoretical gf-values of Kurucz (1994) are seen to be subject occasionally to very large errors, usually overestimates. This can be attributed to the finite size of the Cray computer used in those calculations, which dictated that the number of levels included be truncated, and so upper levels were preferentially omitted from the model atom. Because the sum of the gf-values of transitions arising from a given lower state is normalized to unity, gf-values for the transitions included in the calculation will be overestimated because of the exclusion of others arising from the same level. Thus the calculations will overestimate the gf-value by increasing amounts as the fraction decreases of the actual possible upper states that are included in the atomic model. This fraction decreases to the blue, because higher upper levels are involved for a given lower level. Indeed, the severity of overestimates appears to increase to the blue: all the above changes made to the Kurucz (1994) gf-values were -1.5 or lower below 2650 \AA , but redward of this only one change this negative was required. The overestimates among the Kurucz (1994) Fe I gf-value calculations are thus seen to be due to incompleteness and not to more fundamental difficulties. Undoubtedly many of the weaker mid-UV transitions are missing entirely from the predicted list.

For the hydrides, separate treatment was required, as the lines are naturally associated into bands, and the Kurucz hydride calculations are now several decades old. For OH, the theoretical calculations of Gillis et al. (2001) (communicated in August 2000 by M. Bessell) were used wherever possible. For CH, the LIFBASE data (e.g., Luque & Crosley 1999) were used (communicated in August 2000 by M. Bessell with lines cross-identified). Since these cover only the strongest bands, calculations must still rely on the Kurucz values for the others, notably the 4-3 band of OH with many weak but discernible lines in the Sun. A comparison of the Kurucz OH transition probabilities against those of Gillis et al. (2001) showed strong trends, with discrepancies increasing at high rotation number J . To place them on approximately the same scale, the Kurucz transition probabilities for the OH and CH lines were decreased by an amount $\delta = -0.25 - 0.05 * J_l$ dex. Once missing atomic lines were largely filled in, a comparison was feasible of calculated OH and CH line strengths against those of the Sun and stars. Because solar OH lines were otherwise modeled too strong, all the transition probabilities were reduced by an additional 0.15 dex uniformly. In part because weak OH lines in the Sun were reasonably well modeled but strong ones were still too strong, a chromospheric mitigation of the surface temperature drop was invoked as described shortly. As illustrated below in Figs. 3*d* and *e*, these changes suffice to reproduce both strong and weak 0-0 OH features in stars as well as the Sun.

The calculations were first run using Kurucz (1995) models, but the very metal-poor stars showed a T_{eff} deduced from $\text{H}\alpha$ as much as 200 K higher than that from fitting the mid-UV. That discrepancy was removed by adopting Castelli et al. (1997) models, models in which convective overshoot has been turned off. We did not use the alpha-enhanced Castelli et al. (1997) models, as they are available for only a single value of the alpha-element abundance enhancement.

Like the Kurucz (1995) models, the Castelli et al. (1997) models we used were calculated with $\chi_t = 2 \text{ km s}^{-1}$ and a logarithmic solar iron abundance of -4.37 with respect to the abundance by number of hydrogen plus helium, which amounts to -4.33 with respect to hydrogen alone. These choices are about 1 km s^{-1} higher in χ_t than the $\sim 1 \text{ km s}^{-1}$ typically found for the solar flux spectrum, and about 0.15 dex higher in iron abundance than indicated by the meteoric iron abundance and by several recent determinations for the Sun (e.g., Biéumont et al. 1991; Holweger, Kock, & Bard 1995). Thus both sets of models were calculated with higher line blanketing than expected for a solar-type star of the nominal model metallicity, since iron lines dominate the UV and optical spectrum, and the higher χ_t increases the strengths of moderately strong lines of every species.

For each star including the Sun, a Castelli et al. (1997) model was interpolated to the nearest 50 K in T_{eff} (25 K for the Sun), 0.1 dex in $\log g$, and 0.05 dex in $[\text{Fe}/\text{H}]$. The microturbulent velocity χ_t was changed at all depths to the value indicated for each star in the table and figures below. To minimize the overblanketing effect, our models were interpolated to a nominal grid abundance 0.10 – 0.15 dex lower than that desired. To set abundances, the abundance of the interpolated model was then raised to the desired value and the relative abundance of iron dropped by 0.15 dex. The specific light-element abundance elevations required by the optical observation were adopted, or assumed to be zero for the Sun and α Cen A, and all species equilibria were recalculated. This procedure incorporates the specific χ_t and iron and light-element abundances set for the model in calculating both the ionization and molecular equilibria and the line and continuous opacities for its spectrum. Concerning the model structure, the procedure compensates for the effects of overblanketing due to the high choice of iron abundance, but not for the light-element ratio nor for the microturbulence. We anticipate very mild errors in model colors and temperature structure until spectra become dominated by molecular lines or otherwise are considerably stronger-lined than any of these. The comparison of model and observed colors (§6) bears out this expectation.

For the Sun, a model with $T_{\text{eff}} = 5775 \text{ K}$, $\log g = 4.4$, $[\text{Fe}/\text{H}] = 0$, $[\alpha/\text{Fe}] = 0$, and $\chi_t = 1.0 \text{ km s}^{-1}$, was interpolated in the above way. For HD 128620 = α Cen A we adopted a similarly interpolated model with $T_{\text{eff}} = 5800 \text{ K}$, $\log g = 4.3$, $[\text{Fe}/\text{H}] = +0.15 \text{ dex}$, $[\alpha/\text{Fe}] = 0$, $\chi_t = 1.0 \text{ km s}^{-1}$. While Neuforge-Verheecke & Magain (1997) found $T_{\text{eff}} = 5830 \text{ K}$ and $[\text{Fe}/\text{H}] = 0.25 \text{ dex}$, most other analyses have derived somewhat lower T_{eff} and $[\text{Fe}/\text{H}]$ values. At $T_{\text{eff}} = 5800 \text{ K}$ and $\chi_t = 1.0 \text{ km s}^{-1}$, $[\text{Fe}/\text{H}] = 0.15 \text{ dex}$ provides a better match to the mid-UV spectrum of α Cen A.

Even with the use of Castelli et al. (1997) models interpolated as above, another major type of mismatch persisted in all strong-lined stars: cores of lines formed near the surface appeared

too strong in the calculations, especially in extremely strong mid-UV lines such as those of Mg II and Mg I or Fe II and Fe I. This is definitely not due to wayward gf-values or damping constants, because of the trend seen in the mismatch. Profiles calculated for the strongest lines in the most metal-poor spectra generally matched or were somewhat too high in the core, but were somewhat too low in the core in stars of intermediate line strength, and became too low across the the central ten Ångstroms or more in the strongest-lined stars. (See Fig. 3a below for residual trends of this nature.) As noted above, a related mismatch was seen within the OH spectrum itself: in any given strong-lined spectrum, notably that of the Sun for which the model parameters are extremely well known, weak OH lines were matched at a higher oxygen abundance than strong lines. The possibility discussed in §5 that the solar continuum may be drawn too low would lead to a mismatch of opposite sign. To the extent that the gf-values are reliable, then, this indicates an error in the temperature structure of the model.

The most obvious possibility is a chromosphere, which is not incorporated in flux-constant, static models such as those of SYNTHE. The solar chromosphere, for example, is seen in images of the limb and evident from emission reversals in the cores of strong spectral lines such as Mg II. It is generally modeled by an increase in temperature in relatively shallow layers of the atmosphere (e.g., Fontenla et al. 1999). Any of several non-radiative heating sources extending from the photosphere through the chromosphere into the corona could be responsible (e.g., Schrijver 1995; Schrijver et al. 1999; Sterling 2000).

We consequently changed the temperature of individual points in each interpolated stellar model with $[\text{Fe}/\text{H}] \gtrsim -1.0$, beginning just below the point where the model becomes optically thin at 5000 Å (typically at depth number 51 or 52). (We tried this for the more metal-poor models as well, but the profiles of all the strong lines became much too high near the core, so we left these models as they were.) To best fit both optical and mid-UV spectra simultaneously, we increased the temperature at model depths 28 through 48 by 10, 20, 30, 40, 50, 60, 70, 80, 90, 100, 110, 120, 130, 140, 150, 150, 140, 120, 90, 60, and 30 K respectively. This temperature enhancement may be considered an approximate chromosphere, though it is based entirely on empirical fits of one-dimensional spectral line calculations to observed spectral line profiles. It incorporates neither energy transport considerations nor matches to spatially resolved structures, both of which lie beyond the scope of this work.

5. Matching Mid-UV Spectral Calculations

The degree to which our mid-UV and optical spectral calculations match spectra of real stars is illustrated in the figures. The first three show mid-UV spectra, and the last, optical. Within a figure, panels are ordered by wavelength. Flux (central intensity for the solar mid-UV spectrum) is plotted versus wavelength in air. The spectrum calculated for each star (light line) is plotted on top of that observed (heavy line).

In Figure 1, the global mid-UV fit is shown for the nine stars with absolute fluxes. All spectra have been Gaussian smoothed to a FWHM resolution of 500 (550 for HD 128127 and α Cen A). Each spectrum is displaced vertically by $\sim 20\%$ from the one below. For each star a single mid-UV continuum normalization constant was adopted, as listed on the left. On the right, the HD number of each star appears in bold. Below are found the model-atmosphere parameters adopted for the corresponding calculation: T_{eff} (in K), C wherever the chromosphere was modified as described at the end of §4, $\log g$, $[\text{Fe}/\text{H}]$, χ_t (in km s^{-1}). On the following line appear the values in dex of the light-element abundance enhancements $[\text{Element}/\text{Fe}]$ (in dex), first that of oxygen, then those for Mg, Si, Ca, and Ti. (The latter four are grouped together wherever they are the same.) While the fits are generally good, serious discrepancies are noted in α Cen A at the bottom of the figure near $2550 - 2600 \text{ \AA}$ and $2640 - 2710 \text{ \AA}$, regions of relatively little line absorption in the more metal-poor spectra.

Figure 2 illustrates the effect on mid-UV fits when model parameters are changed somewhat. Two of the stars of Fig. 1 are depicted: the moderately weak-lined HD 94028 (top two spectra) and the rather strong-lined HD 184499 (bottom three). Star and model identifications and normalization constants are indicated as in Figure 1. The lower plot for each star represents its best fit, a replot of that star’s comparison in Figure 1.

Comparing the bottom plot to the middle plot shows the effect for HD 184499 of decreasing $[\text{Mg}/\text{Fe}]$ by 0.3 dex to the solar $[\text{Mg}/\text{Fe}]$ ratio. Although minimized by the adoption of a normalization constant 11% higher, the mismatch is still evident. The strengths of the wings of the strong Mg II doublet at 2800 \AA (and of Mg I at 2852 \AA) are poorly reproduced, as is the overall pseudocontinuum level near and below the bound-free edge of Mg I at 2512 \AA . Similar calculations run for HD 94028 show a more dramatic effect in the Mg II and Mg I line wings, which are weak enough that little renormalization is possible, but a smaller effect near 2512 \AA , where the H^- opacity is dominant because of the reduced magnesium abundance.

Comparing the plot just above the best fit for each star to the best fit itself shows the degeneracy of the mid-UV spectra with respect to a simultaneous change in T_{eff} , $\log g$ and $[\text{Fe}/\text{H}]$ designed to preserve overall line strength and ionization equilibrium. For each plot just above the best fit, T_{eff} was decreased by 100 K, $[\text{Fe}/\text{H}]$ and $\log g$ both concurrently decreased by 0.1 dex, and the spectrum renormalized accordingly. This change is very difficult to detect from fitting the mid-UV slope alone at these metallicities and this resolution. The increased metallicity reduces the blue pseudocontinuum relative to the red at the same time that the increased T_{eff} raises it. The change is marginally detectable in HD 94028 from the mismatch of low-opacity windows, but not in HD 184499 because the overall match is less satisfactory. Such a change does lead to a reduction in the normalization parameter, by 11% for HD 94028 and 17% for HD 184499. In principle this might be detected by other means, but only if $[\text{Mg}/\text{Fe}]$ is properly modeled. For as seen above, taking $[\text{Mg}/\text{Fe}] = 0$ (as in the Kurucz flux distributions) can largely compensate in stars such as HD 184499 that show a light-element enhancement.

Our conclusion, then, is that if the mid-UV normalization constant is treated as a completely free parameter (as here), the mid-UV flux distribution by itself can currently be used to set T_{eff} only in MSTO stars with $[\text{Fe}/\text{H}] \leq -1.5$. While the mid-UV was useful in demonstrating the need for models with no convective overshoot and with an approximate chromosphere, our determinations of T_{eff} for the more metal-rich MSTO stars have relied on the optical spectra instead. We show in Fig. 4 below that the Balmer line profiles and the strengths of other high-excitation lines are well matched in the optical spectra of all stars at the same T_{eff} as the best-fit mid-UV spectrum, and in §5 that model colors match observations as well, so that T_{eff} is indeed very well established here. However, our goal of T_{eff} determination for turnoff stars of all metallicities from mid-UV spectra alone is not yet met. We are not able to calculate the low-opacity windows blueward of 2900 Å accurately enough at near-solar metallicity, as we now demonstrate.

Figure 3 plots at higher resolution and higher scale the same mid-UV spectral comparisons as are shown in Figure 1, plus that of the Sun. Panel *a* shows 2627.5 – 2630.5 Å, dominated by strong lines. The other panels show regions of locally low line blanketing: *b*, 2642.5 – 2645.5 Å; *c*, 2900.0 – 2903.0 Å; *d*, 3082.5 – 3085.5 Å; *e*, 3100.0 – 3103.0 Å. In all plots in Fig. 3, the spectrum of HD 184499 is offset by 30% from that of HD 128620 = α Cen A, which in turn is offset by 50% from that of the Sun, for which 1.0 marks the height of the true continuum. The same normalization constant as in Fig. 1 has been adopted for each stellar spectrum, as was a normalization for the Sun 1.10 times that given in the Kurucz & Avrett (1981) atlas, as noted on the left. Identifications are provided at the top for the strongest lines as calculated in the solar spectrum. Manually added lines are flagged with a colon following the decimal digits of the wavelength in Ångstroms. Next appears the species, the lower excitation potential in eV of atomic transitions or the band and line of molecular ones, the digits following the decimal of the residual flux in the unbroadened line of the solar spectrum calculation, and the log gf-value adopted.

In Fig. 3*e* of the 3100.0 – 3103.0 Å region, calculated and observed spectra agree reasonably well in all stars, including α Cen A and the Sun. No “missing” lines are strong enough to merit explicit identification at the top of the figure. True continuum is reached in each spectrum, but fleetingly, near 3102.5 Å; its placement is sensitive to the treatment of adjacent weak lines. An unblended 0-0 OH line appears at 3101.230 Å, next to a near-continuum high point; both are modeled well in all spectra. The strong atomic lines are well reproduced, as are two moderately strong CH lines at 3100.120 and 3100.170 Å.

Fig. 3*d* offers a further picture of how well both continuum and OH features are modeled. Another continuum window appears near 3084.7 Å, but again with a weak line superimposed in the solar and α Cen A spectra. The relatively unblended OH 0-0 band line at 3084.896 Å, used in several oxygen-abundance investigations, is well reproduced over the factor-of-100 metallicity range of the stars in whose spectra it is detected, including the Sun itself. Nearby at 3085.2 Å is a blend dominated by a stronger 0-0 OH line; it too is reasonably well matched in all stars. Recall that to achieve this agreement, the Gillis et al. (2001) theoretical gf-values for OH were reduced by 0.15 dex; otherwise these features and that of Fig. 2*e*, plus the overwhelming majority of other

OH lines, would be too strong in the Sun. That is, unless the solar continuum were raised.

The solar continuum appears to be well defined, and the OH lines of all bands matched to ~ 0.1 dex, throughout the 3000 – 3100 Å region. Because there are so few continuum windows, however, we cannot rule out a systematic underestimate of the continuum in α Cen A and the Sun of perhaps 5% or 10%. Roughly speaking, raising the α Cen A mid-UV continuum would allow it to be modeled at an [Fe/H] value more consistent with that of Neuforge-Verheeecke & Magain (1997), while raising the solar continuum might eliminate the present need to reduce the theoretical OH gf-values by 0.15 dex. As noted at the end of §6, it would also bring the mid-UV normalization constants of the Sun and α Cen A closer to their expected values. A definite answer could be obtained by deriving the stellar parameters of α Cen A from an optical spectrum in the same way as for the other stars, and from modeling an improved spectrum of the solar near-UV.

Random continuum variations approaching 5% occur for two, and possibly all three, of the stars that were noted in §3 as observed through a smaller aperture. For the continuum seems appropriately placed for all stars in Fig. 3e, but in Fig. 3d the continuum of the HD 106516 observed spectrum appears too low, and in Fig. 3c that of HD 128167 may also be too low. Such variations might also be present in the HD 128620 = α Cen A spectrum as well, but remain undetected because of the difficulty of matching its multitude of lines.

Fig. 3c shows another low-opacity window at 2900 Å. Here the number of missing lines added remains small, and agreement is nearly as good. OH lines are less important, being generally minor constituents of blends. However, windows of true continuum have disappeared from the solar and α Cen A spectra, and are fleeting at best in the echelle spectra of lower resolution that were acquired for mildly metal-poor stars. Continuum placement depends not so much on OH features but rather on whether all missing lines have been spotted. Clearly that is not the case at solar metallicity, where weak missing lines apparently overlap to the extent that they cannot be distinguished as individuals. Although the cumulative effect of their neglect on the total absorption is small, is it significant for the continuum placement, which consequently cannot be determined as well as was the case above from fits such as this. It is placed here and for the remaining panels by adopting the same normalization factors required to match Figs. 3d and e.

By 2645 Å, in Fig. 3b, the fits have deteriorated considerably. This is especially true at and above solar metallicity, where the numbers of missing and identified lines noted at the top are comparable. True continuum still appears in the weakest-lined spectra near the top of the panel, but elsewhere it is gone, lost to a forest of weak lines. Although the fit to the metal-poor stellar spectra is still reasonable, the high-resolution spectra of the α Cen A and the Sun reveal that too few missing lines have been added, often too strong and in the wrong places. For the adjacent region from 2645 to 2700 Å, the sheer number of missing lines precluded their reliable identification at the low resolution of the low-metallicity stellar spectra. Because many were simply omitted, the calculations overestimate the spectral flux in that region – mildly in moderately metal-poor stars but seriously at and above solar metallicity, according to Fig. 1.

From Fig. 3*a*, it is clear that these difficulties are reduced in regions dominated by strong atomic lines. There the fit is dictated more by the ability of the calculations to match the cores and the damping wings of strong lines, and not by modeling the weak or missing features. These are largely suppressed: although the region shown is blueward of that of panel *b*, only one missing line is noted in it. The wings of the strong lines are reproduced well in the four top spectra but begin to be somewhat too broad near the core in HD 106516 and HD 201891. The entire $\pm 1 \text{ \AA}$ about the core is too deep in α Cen A and the Sun. This could perhaps be remedied by continuing the temperature enhancement to shallower surface layers than those indicated in §4.

Figure 4 shows fits to the optical spectra of the Sun and all stars except α Cen A. Identifications are given for the strongest lines in the solar spectrum. Since the optical spectra were not fluxed, the continuum was normalized to unity. The same models were used to calculate the synthetic spectra as in Figures 1 and 2. The wavelength regions in panels *a* – *e* depict a variety of magnesium lines and those of other heavier elements, to illustrate the extent to which the spectral calculations match features of a wide range of excitation, ionization, and strength.

Figure 4*f* shows $H\alpha$, to illustrate the satisfactory choice of T_{eff} . The normalization of the $H\alpha$ profile was aided by its position near the center of an echelle order, and was done by interpolating the normalization functions of the two adjacent orders, centered $\pm 75 \text{ \AA}$ away. This was straightforward, for the $H\alpha$ line is much narrower than this and the continuum is very well defined by a spline fit of low order; moreover, the normalization functions for the adjacent orders were very similar. Note that most absorption lines in this panel are telluric, not stellar, as evidenced by their shift in apparent wavelength from one star to the next.

Included in Fig. 4*f* above the best fit for HD 94028 is the spectrum for the cooler HD 94028 model whose mid-UV spectrum is shown in Fig. 2. This illustrates how the fit to $H\alpha$ deteriorates when models of 100 K lower T_{eff} are adopted. The $H\alpha$ profile is relatively insensitive to gravity in this case: calculations adopting a model that differed from the best-fit model only in having $\log g$ 0.2 dex larger produced a profile that deviated only near 6560 \AA and 6565 \AA , by about the thickness of the heavy line. Similar calculations showed no sensitivity of the $H\alpha$ profile to the chromospheric elevation of temperature, nor to changes of 0.3 dex in iron abundance or light-element ratio. However, Kurucz (1995) models required a T_{eff} 200 K hotter, thanks to their inclusion of convective overshoot.

Panels *a* – *e* of Fig. 4 show that all the optical magnesium features are well matched using the same magnesium abundance and the same model as for the best fit to the mid-UV and to $H\alpha$. Panel *a* plots the region near the very high-excitation Mg II doublet at 4481.2 \AA ; *b*, the ground-state Mg I line at 4571.1 \AA ; *c* and *d*, the Mg *b* lines at 5167.3 , 5172.7 , and 5183.6 \AA ; and *e*, the high-excitation Mg I line at 5711.1 \AA . These panels also demonstrate that the calculations match strengths and profiles of other atomic lines regardless of species, excitation, or strength. Among the lines depicted are Ti I at 5173.7 \AA , Ti II at 5185.9 \AA , ground-state Fe I at 5166.3 \AA , Fe II at 4576.3 \AA , and Si I at 5708.4 \AA . These panels also contain missing features: not modeled at all in the calculations are the

absorption lines seen near 4480.8 Å, 5170.7 Å, and 5181.3 Å. They are not telluric, since they appear at the same position in the stellar spectra, and are especially visible in the two stronger-lined stars.

6. Results and Comparisons

Our results for the parameters of the eight metal-poor turnoff stars analyzed here are listed in columns 12 – 15 of Table 1. The T_{eff} values found for these stars by works cited in §1 are included for reference. Our T_{eff} values are seen to fall in the middle of the range of previous results, preferring neither the hotter nor the cooler values. Unfortunately, the number of stars is too small and the scatter too large for more definitive conclusions.

The reliability of our T_{eff} values is supported by a comparison of model colors to those observed. For each star including the Sun, we interpolated the UBV and $b - y$ colors and V magnitudes calculated by Castelli et al. (1997) to the T_{eff} , $\log g$, and $[\text{Fe}/\text{H}]$ values of each model we used. We have made no reddening corrections, nor any corrections for the temperature enhancement invoked in the more metal-rich models as described at the end of §4. The ninth, tenth, and eleventh columns of Table 1 show the difference in $B - V$, $U - B$, and $b - y$ between the observed and calculated colors for each star. The agreement is extremely good in all colors over the entire metallicity range. The mean difference is -0.010 , -0.018 , and 0.000 mag in $B - V$, $U - B$, and $b - y$ respectively. The standard deviation of an individual difference is 0.010 , 0.026 , and 0.015 mag, marginally larger than typical observational errors alone. The color differences are small even for α Cen A, for which both metallicity and T_{eff} are influential (we interpolated to a model $[\text{Fe}/\text{H}] = +0.05$), and for which we have no optical spectrum and so did not derive parameters. For the other stars, $B - V$ and $b - y$ are sensitive primarily to T_{eff} ; their deviations correspond to ± 45 K with no allowance for observational error. Their observed colors are slightly bluer than those of models, but the size of the differences points to a scale error in T_{eff} of less than 50 K.

We thus estimate an uncertainty of ± 50 K in each T_{eff} determination, from this and the poorer quality evident in Figs. 2 and 4*f* of the fits to mid-UV fluxes and $\text{H}\alpha$ profiles as T_{eff} is increased by 100 K, plus the deterioration of the fit shown in Fig. 4*a* to Mg II . From plots like those of Fig. 4 at other wavelengths, we estimate the uncertainty in $[\text{Fe}/\text{H}]$ to be ± 0.05 dex at fixed T_{eff} , increasing to ± 0.1 dex when the T_{eff} uncertainty is included. The mid-UV slopes and $\text{H}\alpha$ profiles are only weakly sensitive to $\log g$, so our results for $\log g$ are susceptible (as are those of other groups relying on ionization equilibria) to errors in g -value scales and to possible non-LTE effects. We have not yet taken full advantage of the technique of matching damping wings of strong lines, incorporating improved treatments of hydrogen broadening such as those of Anstee & O’Mara (1995) and Barklem & O’Mara (1997). It would be valuable to do so given the constraints this would offer on alternative measurements of the fundamental properties of these standard stars, for example parallaxes from HIPPARCOS and other space missions. However, the following comparisons of observed and model fluxes indicate that the $\log g$ values are good to ± 0.1 dex as they stand.

We first compare the UV normalization constant with that expected. According to Mihalas & Binney (1981), the ratio of observed to emitted stellar flux is $f/F = \theta^2/4$, where the angular diameter $\theta = 2R/D$, R being the stellar radius and D its distance. For each star we calculate $\log R$ in solar units as $0.5(\log M - \log g + 4.4377)$, assuming masses $M = 0.8 M_\odot$ for the metal-poor stars based on stellar isochrones (VandenBerg et al. 2000) and $1.15 M_\odot$ for HD 128167, and adopting $1.16 M_\odot$ for α Cen A as derived from its orbit by Pourbaix et al. (1999). The distance in solar units is found from the parallax, and the theoretical flux normalization constant follows from F/f times 4.2545×10^{10} to convert to square steradians. The ratio of this theoretical constant to that actually used to scale the observations in Figs. 1 and 3 is listed in column 7 of Table 1.

Agreement is good for all stars but one. For α Cen A, the ratio is 0.46, suggesting an observed flux that is too low. Indeed, Linsky & Wood (1996) saw this in their 1995 mid-UV α Cen A HST observations with GHRS: relative to earlier GHRS and IUE observations of α Cen A, “our fluxes are lower (by factors of 5.6 and 4.8 for the Mg II and Fe II spectra, respectively), presumably because of the star’s being misplaced at the edge of the small aperture.” From a visual comparison with Fig. 1 of Linsky & Wood (1996), the fluxes we are using for the Linsky et al. (2000) STIS α Cen A spectrum should be raised by a factor of 2.1. This brings the α Cen A ratio to 0.96, and results in an average of the nine stellar ratios of 1.06 ± 0.05 , with an individual standard deviation of 0.15. For the Sun, the ratio is 0.91 given the scale factor of 1.10 noted above, which is within the stated normalization uncertainty but still low. These α Cen A and solar ratios would be closer to unity were the continuum levels for their spectra drawn higher by 5% – 10%, a possibility raised in §5. As matters stand, errors in continuous opacity are limited to <10% nonetheless.

The apparent V magnitude may also be compared to that expected from the model. From the V magnitudes tabulated with the model colors, we calculated the difference in the stellar model V with respect to the solar model, added this and $5 \log(D/R)$ to the observed solar $V = -26.7$, then subtracted this from the observed stellar V magnitude. Again, no reddening or other corrections were applied. The resulting differences are shown in column 8 of Table 1. The agreement is reasonable: the theoretical magnitudes average 0.09 ± 0.06 mag brighter than those observed, with a ± 0.18 mag individual standard deviation.

7. Summary and Discussion

In brief, we have calculated high-resolution mid-UV spectra from first principles, after modifying line parameters and assigning line identifications for missing lines based on changes seen among spectra of stars spanning a range of well-determined values of T_{eff} , $\log g$, and $[\text{Fe}/\text{H}]$. The resulting calculations provide a good fit for turnoff stars of all metallicities redward of 2900 \AA . Previous discrepancies in fitting the solar pseudocontinuum (noted in §1) are attributed not to missing continuous opacity, which is good to <10% near 3100 \AA , but rather to missing or miscalculated line opacity.

To improve the accuracy of the mid-UV gf-values, damping constants, and line identifications derived here, we have determined temperatures, gravities, microturbulence, and abundances for eight stars by calculating fits to optical as well as UV spectra. For stars more metal-poor than one-thirtieth solar, the fit to the mid-UV spectrum was satisfactory using laboratory lines alone, and can by itself determine T_{eff} . For the more metal-rich stars, lines missing from the laboratory list compromise the goodness of fit of the mid-UV spectrum. A 100 K increase in T_{eff} is seen to be difficult to detect from mid-UV spectra alone, as long as $[\text{Fe}/\text{H}]$ and $\log g$ are increased by 0.1 dex to compensate. This $T_{\text{eff}} - [\text{Fe}/\text{H}]$ degeneracy parallels the age-metallicity degeneracy in elliptical galaxies (Worthey 1994, 1999). As with galaxies, it is reduced here by considering the Balmer lines, with the advantage that stellar models need not include Balmer-line emission nor composite populations. Here T_{eff} was set for stars with $[\text{Fe}/\text{H}] \geq -1.5$ by matching the $\text{H}\alpha$ line profile and the strengths of other high-excitation features.

For all the metal-poor stars, the excellent match between calculations and observations of both optical and mid-UV spectra, and between model and observed colors, indicates an uncertainty of ± 50 K in an individual T_{eff} determination, and a similar uncertainty in the T_{eff} scale. Moreover, the stellar V magnitudes generally agree to 0.1 mag, and the mid-UV normalization constants to 10%, with those expected from the stellar angular diameter found from the observed parallax and the model $\log g$, assuming reasonable masses.

In this process, it was found that these optical diagnostics and the slope of the mid-UV continuum could only be fit simultaneously when using models of Castelli et al. (1997) in which convective overshoot has been turned off. Our work thus agrees with that of Castelli et al. (1997), who found that their models better reproduce the Balmer profiles in the Sun than do those of Kurucz (1995). Downloading the Castelli et al. (1997) models from the Kurucz web site at <http://cfaku5.harvard.edu> is recommended for all work where the results depend upon the temperature structure in deep continuum-forming regions.

Residual discrepancies in fitting the profiles of very strong atomic lines, and the strengths of strong versus weak solar OH lines in the 3000 – 3100 Å region, are reduced here by mimicking a chromosphere towards the surface of every model with $[\text{Fe}/\text{H}] \gtrsim -1$. As described at the end of §4, the model temperature was raised in the region just above the depths where optical continuum and weak lines are formed. While this procedure was necessary to match strong-line cores and OH line strengths over a very broad range of metallicity with a single set of gf-values, it is definitely an oversimplification. Energy and stability considerations remain to be examined. Fits might be improved with a different choice of temperature enhancement. Indeed, a two-stream model might be found necessary. In the meantime, line cores also will be subject to uncertainties due to the presence of chromospheric emission. Peterson & Schrijver (1997) demonstrate that Mg II emission is always present in solar-temperature stars, with a strength that increases with increasing metallicity. Emission also increases with increasing stellar activity (Ayers et al. 1995). Since activity in turn is associated with rapid rotation, stronger Mg II emission appears commonly among young stars and close binaries. Consequently, no single quiescent chromosphere appears capable of modeling the

very core of the profile of a strong line in all turnoff stars.

The reliability of our T_{eff} values and the good match achieved for OH lines enable a second look at the oxygen abundances of metal-poor stars, which are still uncertain as noted in §1. Our values for T_{eff} are intermediate, suggesting that T_{eff} is not the sole cause of the oxygen discrepancies. We defer a more detailed discussion to a future paper by Peterson, Dorman, & Rood (2001), who compare oxygen abundances derived from the OH lines with those from the permitted and forbidden lines of atomic O I in these stars.

The manual addition of lines to the model line list, to match otherwise missing features seen in the observed spectrum, is clearly necessary for even an approximate representation of the mid-UV spectrum of solar-temperature stars of one-tenth solar metallicity and higher. Nonetheless the procedure has its important limitations. One is that as overall line strength increases, the proportion of missing lines goes up dramatically; disentangling them requires a broader range of spectra of high quality, as discussed below. Another is that the excitation or ionization of the transition could be misjudged; the ramifications are discussed in the next paragraph. A third is that many missing lines may not be due to iron as assumed, but to other elements. As discussed in §4, this is potentially serious redward of the bound-free absorption edge of Mg I near 2512 Å. Elsewhere the effect should be minimal, because although other iron-peak elements contribute significant line absorption throughout the mid-UV, the relative abundances of all other iron-peak elements with respect to iron change little from one late F or early G main-sequence star to another in both halo and disk populations in our Galaxy. To be sure, the list generated by this procedure cannot be expected to reproduce the spectrum of a peculiar A or F star, for example a Cr-enhanced star, in which the iron-peak ratio has been dramatically altered (Jaschek & Jaschek 1990).

More generally, the list is not suitable for modeling stars whose parameters lie well outside the range of those analyzed here. In such cases, any difference becomes important between the assigned and the actual excitation (and ionization) potential of the transition responsible for a line, leading to a significant misrepresentation of its strength. Consequently, the present list cannot be expected to reproduce the spectra of stars hotter than early F nor cooler than early G, nor giants, as well as stars of metallicity substantially higher than solar for which lines are still missing. The list could be made suitable for those stellar types by extending the present analysis to include such stars, provided high-resolution, high S/N mid-UV spectra are available in which mismatches induced by errors in the list can be visually identified and corrected. We discuss this further below.

Conversely, the list as it stands should do as well as indicated by Fig. 1 and Fig. 3 in reproducing the mid-UV spectra of any other late F or early G star of solar metallicity or less, provided a suitable model atmosphere is chosen. This holds because once the gf-value and damping constant of a line transition are set, elemental abundance and the Boltzmann and Saha equilibria at each point in the atmosphere fully determine line strength in quiescent stars such as these. Dynamical effects can be ignored, and non-equilibrium effects (if any) are slowly-varying functions of spectral type, hence absorbed into the gf-value determinations. The only exception is the chromospheric emission noted

above. Were the line list improved to the point that a reliable match is achieved to the mid-UV spectra of F and G stars of solar metallicity and above, we could expect to use the mid-UV slope to at least constrain age and metallicity, regardless of its overall level or the appropriate light-element abundance ratio, as these could be incorporated in a grid of calculations covering the entire relevant parameter space.

Spectral indexes offer an alternative means by which mid-UV spectral calculations alone might constrain metallicity and T_{eff} of a star or age of a stellar system. The principle is to construct indexes based on spectral regions dominated by features whose behavior breaks the age/metallicity degeneracy and elucidates the alpha enhancement, examples of which are the Balmer lines and ratios of Fe I/Fe II and Mg I/Mg II line strengths. Spectral indexes have indeed been used as diagnostics of age and metallicity in ellipticals by several of the groups mentioned in §1. For example, Lotz, Ferguson, & Bohlin (2000) have compared mid-UV and optical line indexes they calculated from Kurucz flux distributions against mean values observed for the stars considered by Fanelli et al. (1990). Unfortunately, poor agreement was seen for all but two mid-UV indexes, the slope of the pseudocontinuum between 2600 Å and 3100 Å, and blended absorption near 2538 Å.

We should be able to improve upon some of those index calculations immediately. As Figs. 1 and 3 illustrate, the current spectral calculations should be reasonably reliable at all metallicities in spectral regions redward of 2900 Å, and for those dominated by strong lines blueward of that. This includes several indexes already in use, notably the Mg II and Mg I lines at 2800 Å and 2852 Å and line blends in the 3000+ Å region. We plan to begin such index calculations shortly, and make them generally available.

Blueward of 2900 Å, however, our calculations are not yet reliable enough. Fig. 1 shows that our calculated spectra of solar-metallicity stars substantially overestimate the true fluxes in those wavelength regions not dominated by strong lines. Somewhat ironically, our calculations thus suggest that neither of well-behaved Lotz, Ferguson, & Bohlin (2000) indexes is currently reliable at near-solar metallicity.

The problem undoubtedly is lines still missing from the line list. As seen in Fig. 3, missing lines often overlap in the solar spectrum to such an extent that they could not be individually discerned, and so their species and wavelength assignments became arbitrary. This was true especially in the 2550 – 2600 Å and the 2640 – 2710 Å regions, where we did not complete the process. This is the reason for the excess flux seen in the calculations at solar metallicity in these regions.

This could be remedied were spectra obtained of the same quality as that of α Cen A for stars of the line strength of HD 184499 that span a range of properties, notably T_{eff} . For example, the spectra of HD 184499 and a Hyades F star with $T_{\text{eff}} \sim 6500$ K should have about the same overall line strength: the Hyades star’s higher abundance, $[\text{Fe}/\text{H}] \sim +0.15$, is offset by its higher T_{eff} at the rate of 0.1 dex per 100 K, as Fig. 2 illustrates. Because line crowding is much lower than in α Cen A, comparing high-resolution mid-UV spectra of HD 184499 and a sharp-lined Hyades F star could show where the strongest lines are that are missing at solar metallicity and suggest their identities

from the changes observed with T_{eff} . The α Cen A and solar spectra could then be used to fill in the rest. Analyzing an additional star closer in T_{eff} to HD 184499 but with $[\alpha/\text{Fe}] = 0$ would show explicitly which transitions are due to magnesium in the 2550 Å region, and whether OH has been properly characterized throughout the 2900 – 3100 Å domain.

At that point, the full arsenal of indexes representing the strengths of mid-UV features could be calculated from the spectra, and their behavior with T_{eff} , $\log g$, $[\text{Fe}/\text{H}]$, and $[\alpha/\text{Fe}]$ assessed explicitly. This is a major advantage of calculations from first principles over empirical libraries, which are confined to the spectra of stars available nearby. It is a major goal of this project. Indexes should result with significant diagnostic power for the integrated-light spectrum of an old stellar system.

We are indebted to S. Allen of U. C. Santa Cruz for writing the initial scripts to convert the VAX version of Kurucz codes into UNIX versions. We are grateful to M. Bessell of Mount Stromlo and Siding Spring Observatories for communicating the Gillis et al. (2001) and LIFBASE gf-value calculations and programs for their comparison against the Kurucz values, to J. Valenti of the Space Telescope Science Institute for providing the HD 128620 spectral reductions, to T. Misch of Lick Observatory for obtaining the blue spectrum of HD 114762, and to J. Fulbright of the Dominion Astrophysical Observatory for contributing his optical echelle spectra. We thank Fulbright and R. P. Kraft of Lick Observatory, R. L. Kurucz of the Harvard-Smithsonian Center for Astrophysics, T. M. Lanz and S. R. Heap of the NASA/Goddard Space Flight Center, D. C. Morton of the Herzberg Institute for Astrophysics, and R. W. O’Connell of the University of Virginia for useful discussions. This work has made use of the SIMBAD database, operated at CDS, Strasbourg, France. Support for this work was provided by NASA Astrophysics Data Program contract S-92512-Z, STScI grants GO-07395, GO-07402, and AR-8371, and NSF grants AST 99-00582 and AST-0098725, to Astrophysical Advances, and by NASA ADP grant NAG 5-7104, NASA LTSA grant NAG 5-6403, and STScI grant GO-06607 to the University of Virginia.

REFERENCES

- Allende Prieto, C., & Lambert, D. L. 2000, *AJ*, 119, 2445
- Allen, C. W. 1973, *Astrophysical Quantities*, 3rd. ed. (London: Athlone), 162
- Alonso, A., Arribas, S., & Martinez-Roger, C. 1996, *A&A*, 313, 873
- Anstee, S. D., & O’Mara, B. J. 1995, *MNRAS*, 276, 859
- Ayres, T. D., et al. 1995, *ApJS*, 96, 223
- Balachandran, S. C. 2000, in *Proc. IAU JD8*, in press
- Balachandran, S., & Bell, R. 1998, *Nature*, 392, 791

- Barklem, P. S., & O'Mara, B. J. 1997, MNRAS, 290, 102
- Biémont, E., Badoux, M., Kurucz, R. L., Ansbacher, W., & Pinnington, E. H. 1991, A&A, 249, 539
- Blackwell, D. E., Petford, A. D., Shallis, M. J., & Simmons, G. J. 1982, MNRAS, 199, 43
- Blackwell, D. E., & Lynas-Gray, A. E. 1998, A&AS, 129, 505
- Boesgaard, A. M., King, J. R., Deliyannis, C. P., & Vogt, S. S. 1999, AJ, 117, 492
- Butler, et al. 1993, J. Phys. B, 26, 4409
- Carney, B. W., Latham, D. W., Laird, J. B., & Aguilar, L. A. 1994, AJ, 107, 2240
- Castelli, F., Gratton, R. G., & Kurucz, R. L. 1997, A&A, 318, 841
- Chmielewski, Y., Friel, E., Cayrel de Strobel, G., & Bentolila, C. 1992, A&A, 263, 219
- Dorman, B., Rood, R. T., & O'Connell, R. W. 1993, ApJ, 419, 596
- Fanelli, M. N., O'Connell, R. W., Burstein, D., & Wu, C.-C. 1990, ApJ, 364, 272
- Fontenla, J., White, O. R., Fox, P. A., Avrett, E. H., & Kurucz, R. L. 1999, ApJ, 518, 480
- Fuhr, J. R., Martin, G. A., & Wiese, W. L. 1988, J. Phys. Chem. Ref. Data, 17, Suppl. 4
- Fuhrmann, K., Axer, M., & Gehren, T. 1994, A&A, 282, 585
- Fullbright, J. P. 2000, AJ, 120, 1841
- Furenlid, I., & Meylan, T. 1990, ApJ, 350, 827
- Gillis, J. R., Goldman, A., Stark, G., & Rinsland, C. P. 2001, J. Quan. Sp. Rad. Transfer, 68, 225
- Gratton, R. G., Carretta, E., & Castelli, F. 1996, A&A, 314, 191
- Heap, S. R., et al. 1998, ApJ, 492, L131
- Henry, R. B. C., & Worthey, G. 1999, PASP, 111, 919
- Holweger, H., Kock, M., & Bard, A. 1995, A&A, 296, 233
- Israelian, G., Rebolo, R., García López, R. J., Bonifacio, P., Molaro, P., Basri, G., & Shchukina, N. 2000, ApJ, 551, 833
- Jaschek, C., & Jaschek, M. 1990, *The Classification of Stars* (Cambridge: Cambridge Univ. Press)
- King, J. R. 1993, AJ, 106, 1206

- Kraft, R. P. 2000, in Proc. IAU 2000, JD8, in press
- Kurucz, R. L. 1994, CD-ROM 22, Atomic Data for Fe and Ni (Cambridge: Smithsonian Astrophys. Obs.)
- Kurucz, R. L. 1995, in A.S.P. Conf. Ser. 81, *Laboratory and Astronomical High Resolution Spectra*, ed. A. J. Sauval, R. Blomme, & N. Grevesse (San Francisco: ASP), 583
- Kurucz, R. L., & Avrett, E. H. 1981, “Solar spectrum synthesis. I. A sample atlas from 224 to 300 nm”, S.A.O. Spec. Rpt., 391
- Kurucz, R. L., & Bell, B. 1995, Kurucz CD-ROM No. 23 (Cambridge, MA: Smithsonian Astrophysical Observatory)
- Kurucz, R. L., Furenlid, I., Brault, J., & Testerman, L. 1984, Solar Flux Atlas from 296 to 1300 nm (Sunspot, NM: National Solar Obs.), available from <http://cfaku5.harvard.edu>
- Lambert, D. L. 2000, in Proc. IAU 2000, JD8, in press
- Lejeune, T., Cuisinier, F., & Buser, R. 1997, A&AS, 125, 229
- Linsky, J. L., Pagano, I., Valenti, J., & Gagne, M. 2000, in *Cool Stars, Stellar Systems and the Sun: Eleventh Cambridge Workshop*, ed. García López, R. J., Rebolo, R., & Zapatero Osorio, M., A. S. P. Conf. Ser., 223, in press
- Linsky, J. L., & Wood, B. E. 1996, ApJ, 463, 254
- Lombardi, G. G., Smith, P. L., & Parkinson, W. H. 1981, Phys. Rev. A, 24, 326
- Lotz, J. M., Ferguson, H. C., & Bohlin, R. C. 2000, ApJ, 532, 830
- Luque, J., & Crosley, D. R. 1999, App. Opt., 38, 1423, available from <http://www.sri.com/CEM/LIFBASE>
- Magain, P. 1984, A&A, 132, 208
- McWilliam, A., Preston, G. W., Sneden, C. & Searle, L. 1995, AJ, 109, 2757
- Mihalas, D., & Binney, J. 1981, *Galactic Astronomy*, 2nd. ed. (San Francisco: W. H. Freeman), 93 – 96
- Morton, D. C. 1991, ApJS, 77, 119
- Nave, G., Johansson, S., Axner, O., Ljungberg, P., Malmsten, Y., & Baschek, B. 1994, Physica Scripta, 49, 581
- Neuforge-Verheecke, C., & Magain, P. 1997, A&A, 328, 261
- Nissen, P. E., Chen, Y. Q., Schuster, W. J., & Zhao, G. 2000, A&A, 343, 722

- O'Brian, T. R., Wickliffe, M. E., Lawler, J. E., Whaling, W., & Brault, J. W. 1991, *J. Opt. Soc. Amer. B*, 8, 1185
- O'Connell, R. W. 1976, *ApJ*, 206, 370
- Peterson, R. C. 1976, *ApJ*, 210, L123
- Peterson, R. C. 2000, in *Proc. IAU 2000, JD8*, in press
- Peterson, R. C., Dalle Ore, C. M., & Kurucz, R. L. 1993, *ApJ*, 404, 333
- Peterson, R. C., Dorman, B., & Rood, R. T. 2001, in preparation
- Peterson, R. C., & Schrijver, C. J. 1997, *ApJ*, 480, L47
- Peterson, R. C., & Schrijver, C. J. 2000, *Cool Stars, Stellar Systems and the Sun: Eleventh Cambridge Workshop*, ed. García López, R. J., Rebolo, R., & Zapatero Osorio, M., *A. S. P. Conf. Ser.*, 223, in press
- Ponder, J. M., et al. 1998, *AJ*, 116, 2297
- Pourbaix, D., Neuforge-Verheecke, C., & Noels, A. 1999, *A&A*, 344, 172
- Prochaska, J. X., & McWilliam, A. 2000, *ApJ*, 537, L57
- Reid, I. N. 1998, *AJ*, 115, 204
- Schrijver, C. J. 1995, *Astronomy and Astrophysics Review*, 6, 181
- Schrijver, C. J., et al. 2000, *Solar Phys.*, 187, 261
- Spinrad, H., Dey, A., Stern, D., Dunlop, J., Peacock, J., Jimenez, R., & Windhorst, R. 1997, *ApJ*, 484, 581
- Spite, M., Francois, P., Nissen, P. E., & Spite, F. 1996, *A&A*, 307, 172
- Sterling, A. C. 2000, *Solar Phys.*, 196, 79
- Thévenin, F., & Idiart, T. P. 1999, *ApJ*, 521, 753
- VandenBerg, D. A., & Bell, R. A. 2000, *Proc. IAU 2000, JD8*, in press.
- VandenBerg, D. A., Swenson, F. J., Rogers, F. J., Iglesias, C. A. & Alexander, D. R. 2000, *ApJ*, 532, 430
- Vogt, S. S. 1987, *PASP*, 99, 1214
- Wheeler, J. C., Sneden, C., & Truran, J. W., Jr. 1989, *ARA&A*, 27, 279
- Worthey, G. 1994, *ApJS*, 95, 107

Worthey, G. 1999, A.S.P. Conf. Ser., 192, 283

Worthey, G., Faber, S. M., & González, J. J. 1992, ApJ, 398, 69

Fig. 1.—

Plots are shown comparing observed (heavy line) and calculated (light line) spectra for the nine stars with fluxed mid-UV spectra included in this study. To the right, the name of each star in bold is accompanied by the model parameters used for the corresponding calculation. At the left is the mid-UV normalization constant for each comparison.

Fig. 2.—

Plots as in Fig. 1 are shown comparing the fits for two stars with small changes in model parameters.

Fig. 3.—

The same as Fig. 1, but on a larger scale in 3 \AA spectral regions. At the bottom is the Sun: two scans of the center of the solar disk are superimposed. At the very top, the strongest lines in the solar spectrum calculation are identified as described in the text. The same mid-UV normalization constants as in Fig. 1 are adopted for the top nine stars. *a)* $2627.5 - 2630.5 \text{ \AA}$. *b)* $2642.5 - 2645.5 \text{ \AA}$. *c)* $2900 - 2903 \text{ \AA}$. *d)* $3082.5 - 3085.5 \text{ \AA}$. *e)* $3100 - 3103 \text{ \AA}$.

Fig. 4.—

Comparisons as in Fig. 1 are shown for optical spectral regions containing magnesium or Balmer lines in eight of the stars plus the Sun. Each observed spectrum (heavy line) has been normalized to unity as described in the text. Line identifications as described for Fig. 3 are shown for the strongest lines in the solar calculation. *a)* Mg II. *b)* Low-excitation Mg I. *c), d)* The Mg b lines. *e)* High-excitation Mg I. *f)* H α . In this panel only, the third plot from the top represents a non-optimal choice of model parameters. It illustrates the degradation of the fit to H α when a T_{eff} is chosen 100 K cooler than that of the plot immediately below.

Table 1. **Stellar Observations, Model Parameters, and Effective Temperatures**

HD	⇐	Observed				⇒	Mid-UV	⇐	Observed – Model			⇒	⇐	Model		⇒	K93	C+94	A+96	G+96	BL98	F00
	V	$B - V$	$U - B$	$b - y$	π	Ratio	V	$B - V$	$U - B$	$b - y$	T_{eff}	$\log g$	[Fe/H]	χ_t	T_{eff}	T_{eff}	T_{eff}	T_{eff}	T_{eff}	T_{eff}	T_{eff}	
19445	+8.06	0.45	-0.25	0.349	25.85	1.37	-0.04	-0.01	-0.01	-0.005	6050	4.5	-2.00	1.0	6007	5842	6050	6066	...	5825		
84937	+8.33	0.39	-0.22	0.303	12.44	1.21	+0.09	-0.01	-0.01	-0.011	6300	4.0	-2.20	1.5	6314	6220	...	6350	6202	6375		
94028	+8.22	0.47	-0.18	0.343	19.23	1.07	+0.25	+0.00	+0.00	-0.005	6050	4.2	-1.40	1.3	6047	5898	...	6060	5998	5900		
106516	+6.11	0.45	-0.14	0.317	44.34	0.99	-0.09	-0.01	-0.03	-0.004	6250	4.3	-0.65	1.0	6221	6118	6208	6267	6233	6200		
114762	+7.31	0.53	-0.06	0.365	24.65	0.96	+0.30	-0.02	+0.01	-0.008	5850	4.0	-0.90	1.0	...	5790	...	5941	5904	5800		
128167	+4.46	0.36	-0.08	0.254	64.66	0.92	-0.05	+0.01	-0.01	+0.008	6850	4.3	-0.35	2.0	6707	6734	6737	...		
128620	+0.00	0.67	+0.23	0.438	742.2	0.46	-0.06	+0.00	+0.01	+0.037	5800	4.3	+0.15	1.0		
184499	+6.62	0.58	+0.00	0.390	31.29	1.11	+0.02	-0.02	-0.02	+0.001	5750	4.0	-0.60	1.2	5734	5726	5750	5750	5773	5700		
201891	+7.37	0.51	-0.17	0.358	28.26	0.92	+0.40	-0.02	-0.07	-0.008	5900	4.1	-1.00	1.0	6014	5817	...	5974	5918	5825		
Sun	-26.7	0.65	+0.13	0.91	...	-0.01	-0.04	...	5775	4.44	+0.00	1.0		

Note. — Units: π in $10^{-3}''$; T_{eff} in K; χ_t in km s^{-1} . Sources: For all stars but HD 128620 = α Cen A, V , $B - V$, and $U - B$ from Carney et al. (1994); $b - y$ from King (1993), except $b - y$ for HD 114762, HD 128167, and HD 201891 from SIMBAD; π from SIMBAD. HD 128620 = α Cen A: V , $U - B$, $b - y$, and π from SIMBAD; $B - V$ from Furenlid & Meylan (1990). All solar observations from Allen (1973). Other T_{eff} sources: K93, King (1993); C+94, Carney et al. (1994); A+96, Alonso, Arribas, & Martinez-Roger (1996); G+96, Gratton, Carretta, & Castelli (1996); BL98, Blackwell & Lynas-Gray (1998); F00, Fulbright (2000).

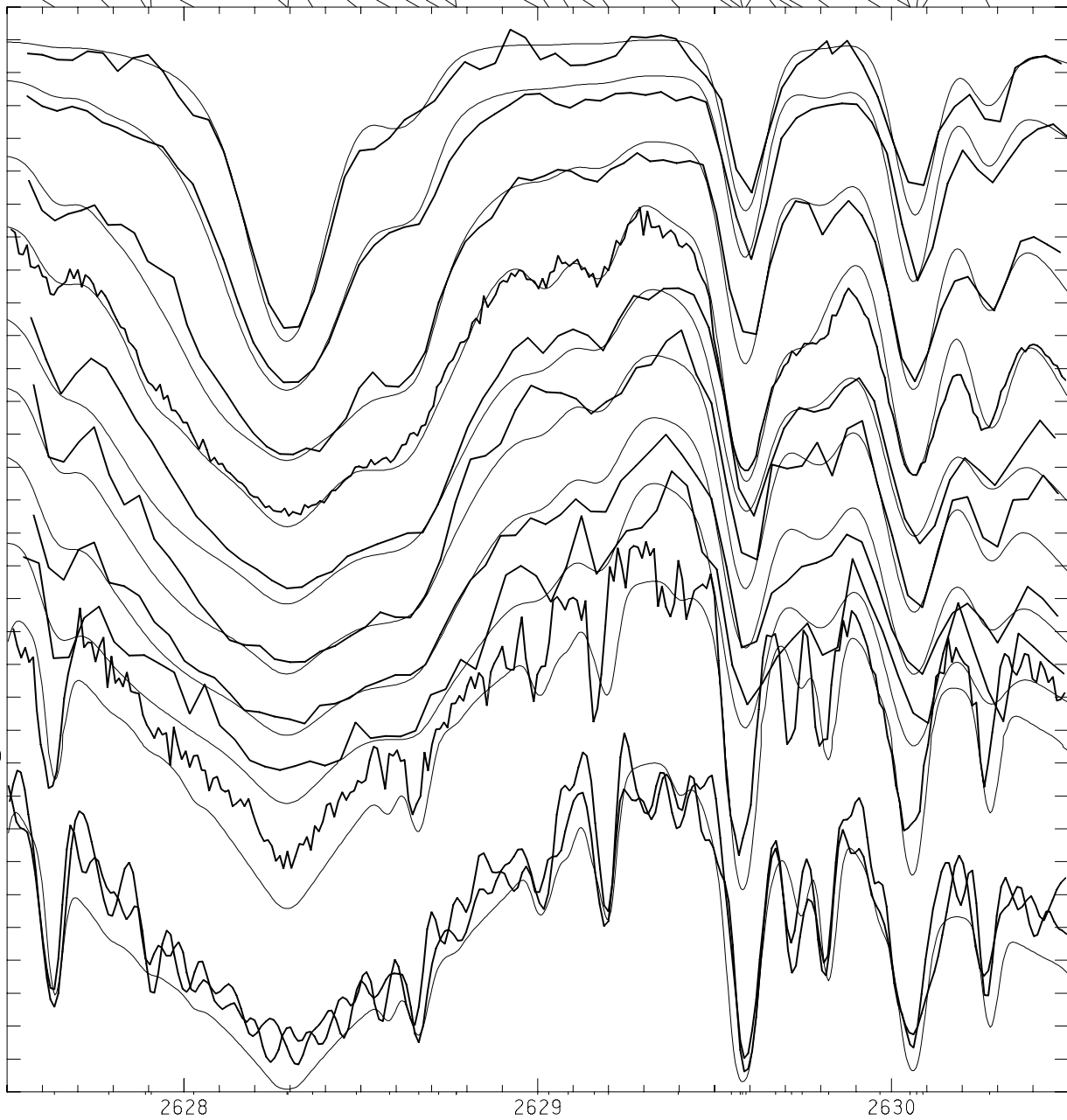
This figure "fig1.gif" is available in "gif" format from:

<http://arxiv.org/ps/astro-ph/0009208v3>

This figure "fig2.gif" is available in "gif" format from:

<http://arxiv.org/ps/astro-ph/0009208v3>

SCALE 1.10 5.26E+15 8.25E+17 1.54E+18 1.53E+18 9.18E+17 3.24E+17 3.60E+18 3.10E+18 4.78E+18



634 Co I 0.43 25 -1.51
 787 OH 2-0 70662 -3.55
 891 Mn I 2.16 399 -1.79
 27 Pt I 0.10 90 -0.56
 907 CrII 6.15 247 0.39

294 FeII 0.12 0 -0.45 291 MnII 5.57 263 0.11
 364 OH 2-0 50722 -3.68

488 Fe I 2.56 778 -3.84
 581 FeII 3.23 34 -1.81
 664 Mg I 2.71 22 -2.30
 720 CrII 6.14 771 -0.63
 770 CoII 3.03 356 -1.27 770 MnII 5.55 530 -0.40

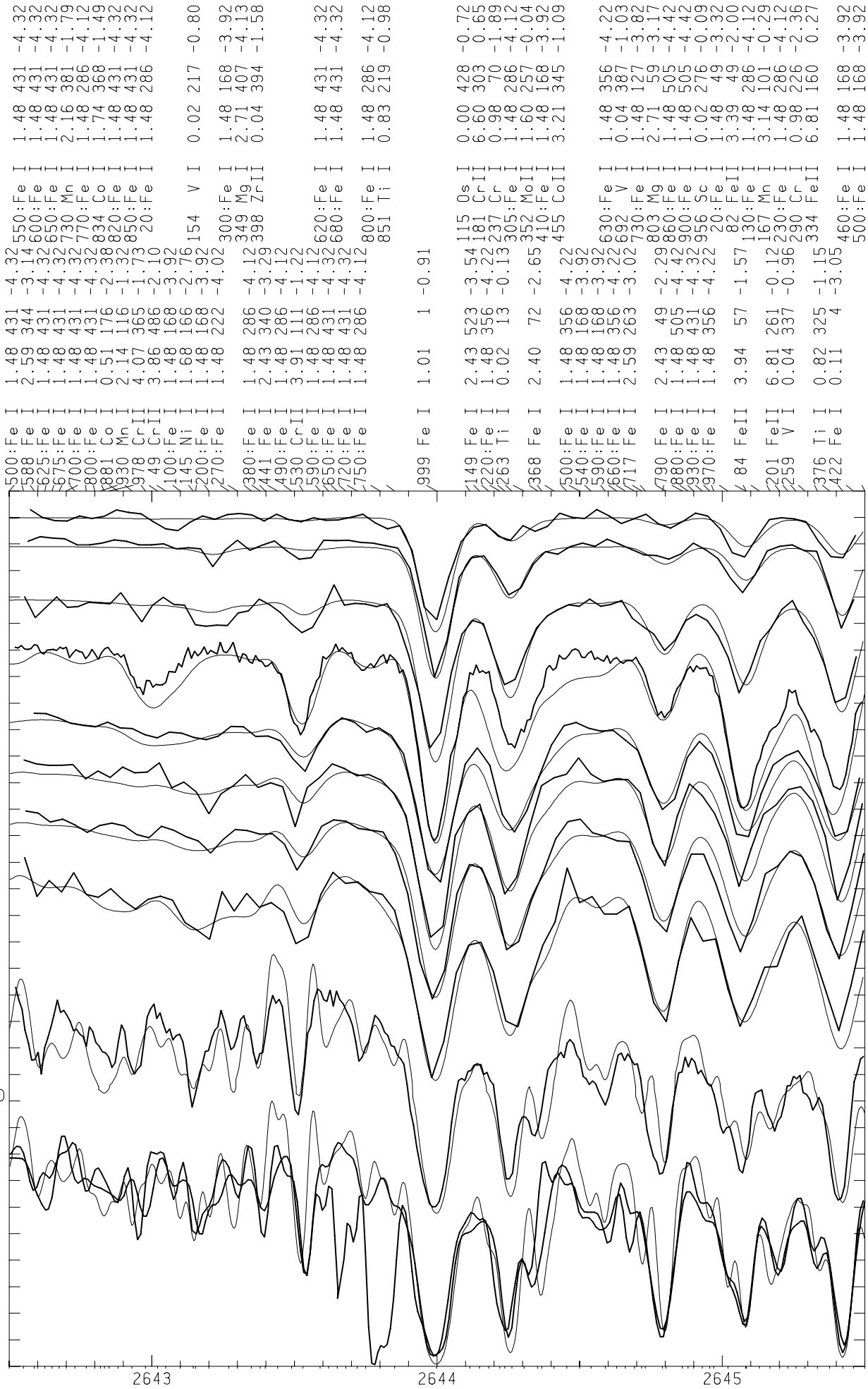
0 Fe I 1.56 209 -3.93
 31 CrII 4.07 204 -1.42
 86 V I 1.05 524 -0.24
 160 FeII 3.23 234 -3.33
 200 Mn I 3.13 73 -0.10

398 CrII 6.18 681 -0.41
 548 FeII 6.72 776 -1.27 572 Fe I 0.12 2 -2.65
 579 CrII 4.29 166 -1.10 589 FeII 2.84 4 -0.29
 673 VII 4.40 729 0.42
 718 CrII 4.07 320 -1.66 747 FeII 2.89 91 -3.14
 823 Cr I 1.00 33 -1.27

968 Co I 1.88 247 -1.18
 52 Mg I 2.71 18 -2.13 53 Mg I 2.71 12 -1.82
 71 FeII 2.86 6 -0.75 89 TiII 3.82 614 -0.76
 278 NiII 1.68 17 -2.25

84937 6300 4.0 -2.20 1.5
 0.9 MgSiCaTi.35
 19445 6050 4.5 -2.00 1.0
 0.8 MgSiCaTi.35
 94028 6050 4.2 -1.40 1.3
 0.5 Mg.35SiCaTi.3
 128167 6850 4.3 -0.35 2.0
 0.0 MgSiCaTi.0
 106516 6250 4.3 -0.65 1.0
 0.3 Mg.25SiCaTi.2
 201891 5900 4.1 -1.00 1.0
 0.2 Mg.25SiCaTi.2
 114762 5850 4.0 -0.90 1.0
 0.2 Mg.3 SiCaTi.2
 184499 5750 4.0 -0.60 1.2
 0.1 Mg.3 SiCaTi.25
 128620 5800 4.3 0.15 1.0
 0.0 MgSiCaTi.0
 SUN - CENTER
 5775 4.4 0.00 1.0
 0.0 MgSiCaTi.0

SCALE 1.10 5.26E+15 8.25E+17 1.54E+18 1.53E+18 9.18E+17 3.24E+17 3.60E+18 3.10E+18 4.78E+18



500:Fe I	1.48 431	-4.32	550:Fe I	1.48 431	-4.32
588:Fe I	2.59 344	-3.14	600:Fe I	1.48 431	-4.32
625:Fe I	1.48 431	-4.32	650:Fe I	1.48 431	-4.32
675:Fe I	1.48 431	-4.32	730:Mn I	2.16 381	-1.79
700:Fe I	1.48 431	-4.32	770:Fe I	1.48 286	-4.12
800:Fe I	1.48 431	-4.32	834:Co I	1.74 368	-1.49
881:Co I	0.51 176	-2.38	820:Fe I	1.48 431	-4.32
930:Mn I	2.14 116	-1.32	850:Fe I	1.48 431	-4.32
978:Cr II	4.07 365	-1.73	20:Fe I	1.48 286	-4.12
49:Cr II	3.86 486	-2.10			
100:Fe I	1.48 168	-3.92			
145:Ni I	1.68 166	-2.76	154 V I	0.02 217	-0.80
200:Fe I	1.48 168	-3.92			
270:Fe I	1.48 222	-4.02	300:Fe I	1.48 168	-3.92
			349:Mg I	1.48 286	-4.12
380:Fe I	1.48 286	-4.12	398:Zn II	2.71 407	-4.13
441:Fe I	2.43 340	-3.29			
490:Fe I	1.48 286	-4.12			
530:Cr II	3.91 111	-1.22			
590:Fe I	1.48 286	-4.12	620:Fe I	1.48 431	-4.32
650:Fe I	1.48 431	-4.32	680:Fe I	1.48 431	-4.32
720:Fe I	1.48 431	-4.32	800:Fe I	1.48 286	-4.12
750:Fe I	1.48 286	-4.12	851 Ti I	0.83 219	-0.98
999 Fe I	1.01 1	-0.91			
1149 Fe I	2.43 523	-3.54	115 Os I	0.00 428	-0.72
220:Fe I	1.48 356	-4.22	181 Cr II	6.00 303	0.65
263 Ti I	0.02 13	-0.13	305:Fe I	0.98 70	-1.89
			352 Mo II	1.48 286	-4.12
368 Fe I	2.40 72	-2.65	410:Fe I	1.60 257	-0.04
			455 Co II	1.48 168	-3.92
500:Fe I	1.48 356	-4.22			
540:Fe I	1.48 168	-3.92	630:Fe I	1.48 356	-4.22
590:Fe I	1.48 168	-3.92	730:Fe I	0.04 387	-1.03
660:Fe I	1.48 356	-4.22	803 Mg I	1.48 127	-3.82
717 Fe I	2.59 263	-3.02	860:Fe I	2.71 59	-3.17
790 Fe I	2.43 49	-2.29	900:Fe I	1.48 505	-4.42
880:Fe I	1.48 505	-4.42	956 Sc I	1.48 505	-4.42
930:Fe I	1.48 431	-4.32	20:Fe I	0.02 276	-0.09
970:Fe I	1.48 356	-4.22	82 Fe II	1.48 49	-3.32
			130:Fe I	3.39 49	-2.00
184 Fe II	3.94 57	-1.57	167 Mn I	1.48 286	-4.12
201 Fe II	6.81 261	-0.12	230:Fe I	3.14 101	-0.29
259 V I	0.04 337	-0.96	290 Cr I	1.48 286	-4.12
			334 Fe II	0.98 226	-2.36
376 Ti I	0.82 325	-1.15	460:Fe I	6.81 160	0.27
422 Fe I	0.11 4	-3.05	500:Fe I	1.48 168	-3.92

84937
6300 4.0 -2.20 1.5
0.9 MgSiCaTi.35

19445
6050 4.5 -2.00 1.0
0.8 MgSiCaTi.35

94028
6050 4.2 -1.40 1.3
0.5 Mg.35SiCaTi.3

128167
6850 4.3 -0.35 2.0
0.0 MgSiCaTi.0

106516
6250 4.3 -0.65 1.0
0.3 Mg.25SiCaTi.2

201891
5900 4.1 -1.00 1.0
0.2 Mg.25SiCaTi.2

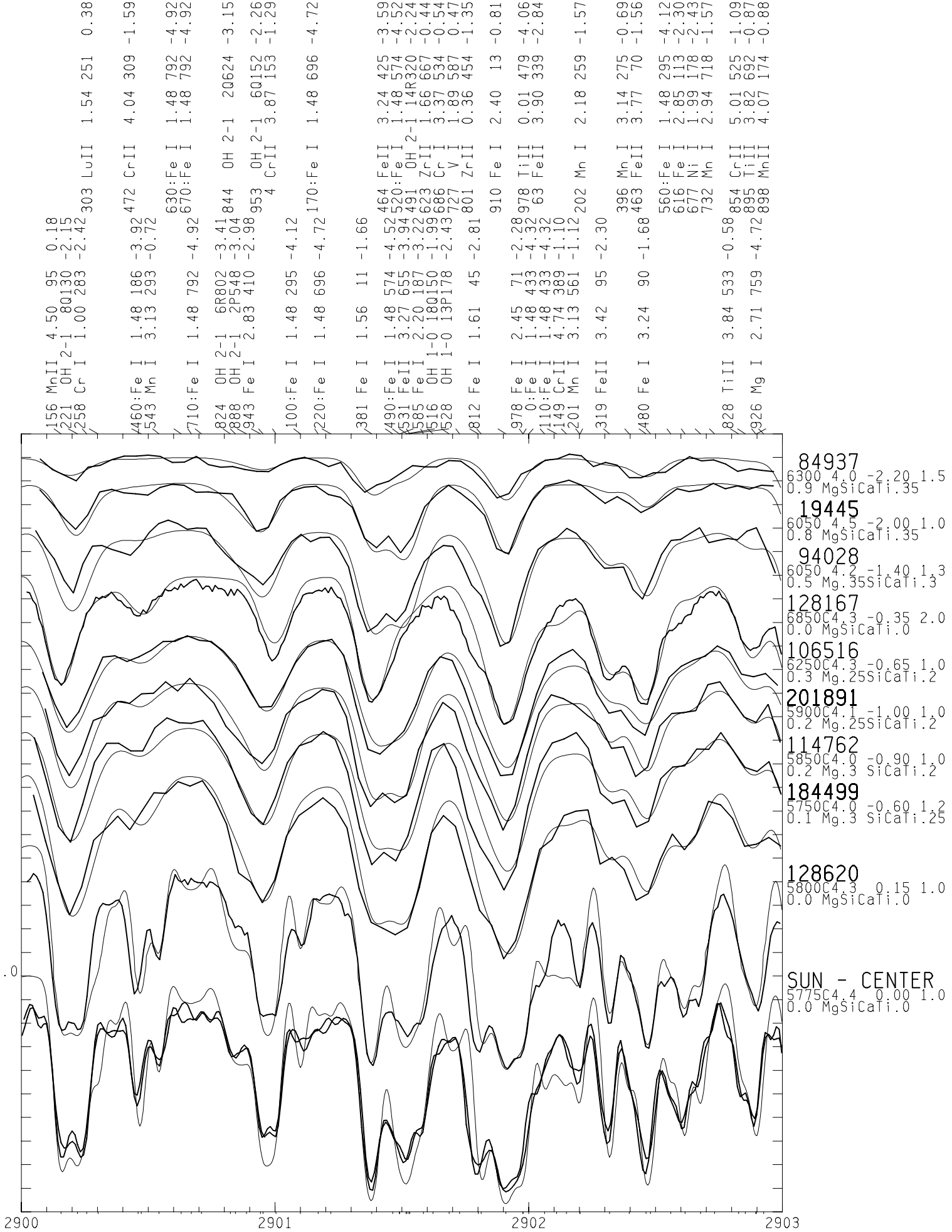
114762
5850 4.0 -0.90 1.0
0.2 Mg.3 SiCaTi.2

184499
5750 4.0 -0.60 1.2
0.1 Mg.3 SiCaTi.25

128620
5800 4.3 0.15 1.0
0.0 MgSiCaTi.0

SUN - CENTER
5775 4.4 0.00 1.0
0.0 MgSiCaTi.0

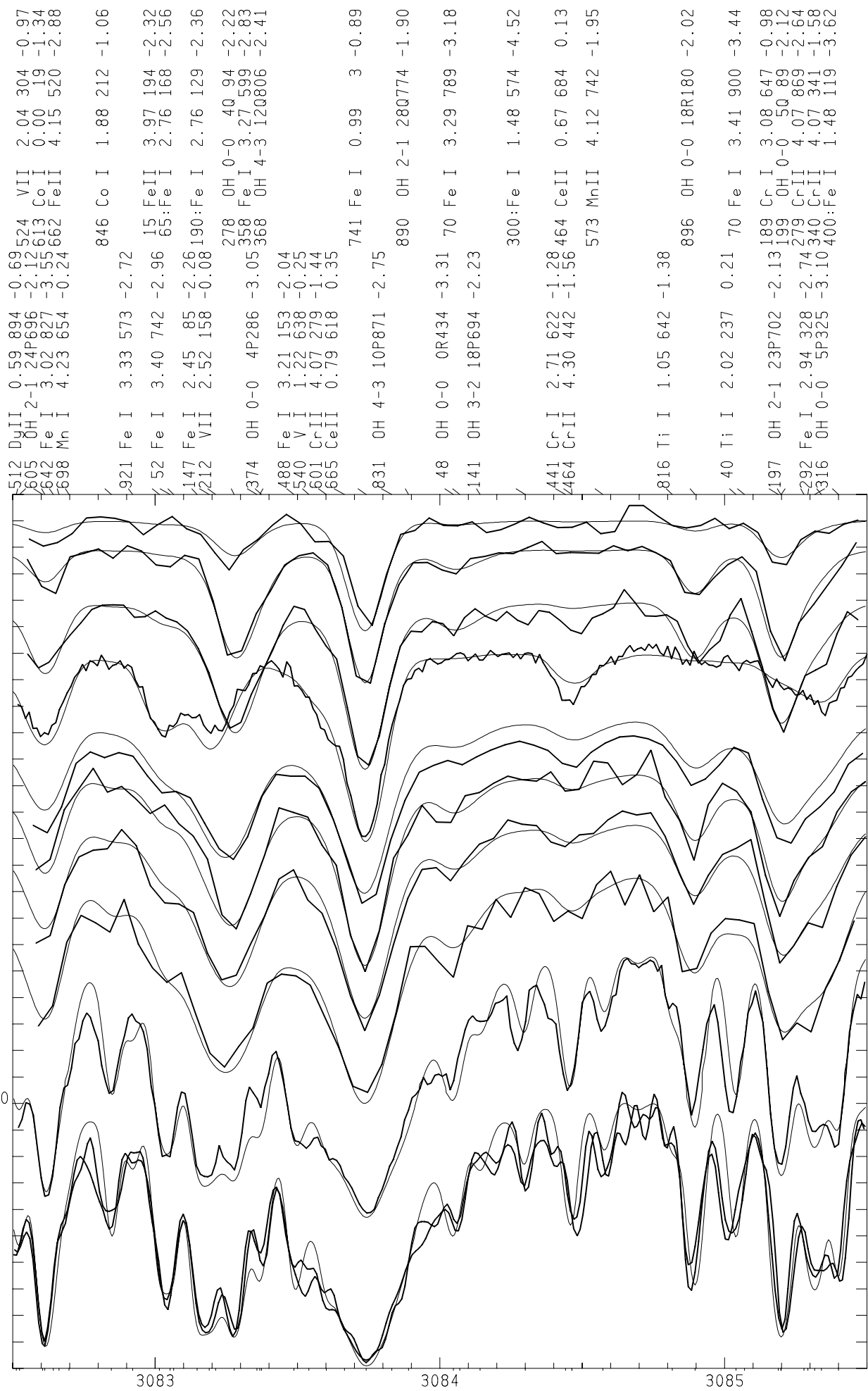
SCALE 1.10 5.26E+15 8.25E+17 1.54E+18 1.53E+18 9.18E+17 3.24E+17 3.60E+18 3.10E+18 4.78E+18



156 MnII 4.50 95 0.18
 221 OH 2-1 80130 -2.15
 258 Cr I 1.00 283 -2.42 303 LuII 1.54 251 0.38
 460:Fe I 1.48 186 -3.92 472 CrII 4.04 309 -1.59
 543 Mn I 3.13 293 -0.72
 710:Fe I 1.48 792 -4.92 630:Fe I 1.48 792 -4.92
 670:Fe I 1.48 792 -4.92
 824 OH 2-1 6R802 -3.41 844 OH 2-1 20624 -3.15
 898 OH 2-1 2P548 -3.04
 943 Fe I 2.83 410 -2.98 953 OH 2-1 60152 -2.26
 4 CrII 3.87 153 -1.29
 100:Fe I 1.48 295 -4.12
 220:Fe I 1.48 696 -4.72 170:Fe I 1.48 696 -4.72
 381 Fe I 1.56 11 -1.66
 490:Fe I 1.48 574 -4.52 520:Fe I 3.24 425 -3.59
 531 FeII 3.27 655 -3.94 491 OH 2-1 14R320 -2.24
 585 Fe I 2.20 187 -3.22 623 ZrII 1.66 667 -0.44
 6516 OH 1-0 18Q150 -1.99 686 Cr I 3.37 534 -0.54
 628 OH 1-0 13P178 -2.43 727 V I 1.89 587 0.47
 812 Fe I 1.61 45 -2.81 801 ZrII 0.36 454 -1.35
 910 Fe I 2.40 13 -0.81
 978 Fe I 2.45 71 -2.28 978 TiII 0.01 479 -4.06
 0:Fe I 1.48 433 -4.32 63 FeII 3.90 339 -2.84
 110:Fe I 1.48 433 -4.32
 149 CrII 4.74 389 -1.10
 201 Mn I 3.13 561 -1.12 202 Mn I 2.18 259 -1.57
 319 FeII 3.42 95 -2.30
 480 Fe I 3.24 90 -1.68 396 Mn I 3.14 275 -0.69
 463 FeII 3.77 70 -1.56
 560:Fe I 1.48 295 -4.12
 616 Fe I 2.85 113 -2.30
 677 Ni I 1.99 178 -2.43
 732 Mn I 2.94 718 -1.57
 828 TiIII 3.84 533 -0.58 854 CrII 5.01 525 -1.09
 895 TiII 3.82 692 -0.87
 926 Mg I 2.71 759 -4.72 898 MnII 4.07 174 -0.88

84937
 6300 4.0 -2.20 1.5
 0.9 MgSiCaTi.35
 19445
 6050 4.5 -2.00 1.0
 0.8 MgSiCaTi.35
 94028
 6050 4.2 -1.40 1.3
 0.5 Mg.35SiCaTi.3
 128167
 6850 4.3 -0.35 2.0
 0.0 MgSiCaTi.0
 106516
 6250 4.3 -0.65 1.0
 0.3 Mg.25SiCaTi.2
 201891
 5900 4.1 -1.00 1.0
 0.2 Mg.25SiCaTi.2
 114762
 5850 4.0 -0.90 1.0
 0.2 Mg.3 SiCaTi.2
 184499
 5750 4.0 -0.60 1.2
 0.1 Mg.3 SiCaTi.25
 128620
 5800 4.3 0.15 1.0
 0.0 MgSiCaTi.0
 SUN - CENTER
 5775 4.4 0.00 1.0
 0.0 MgSiCaTi.0

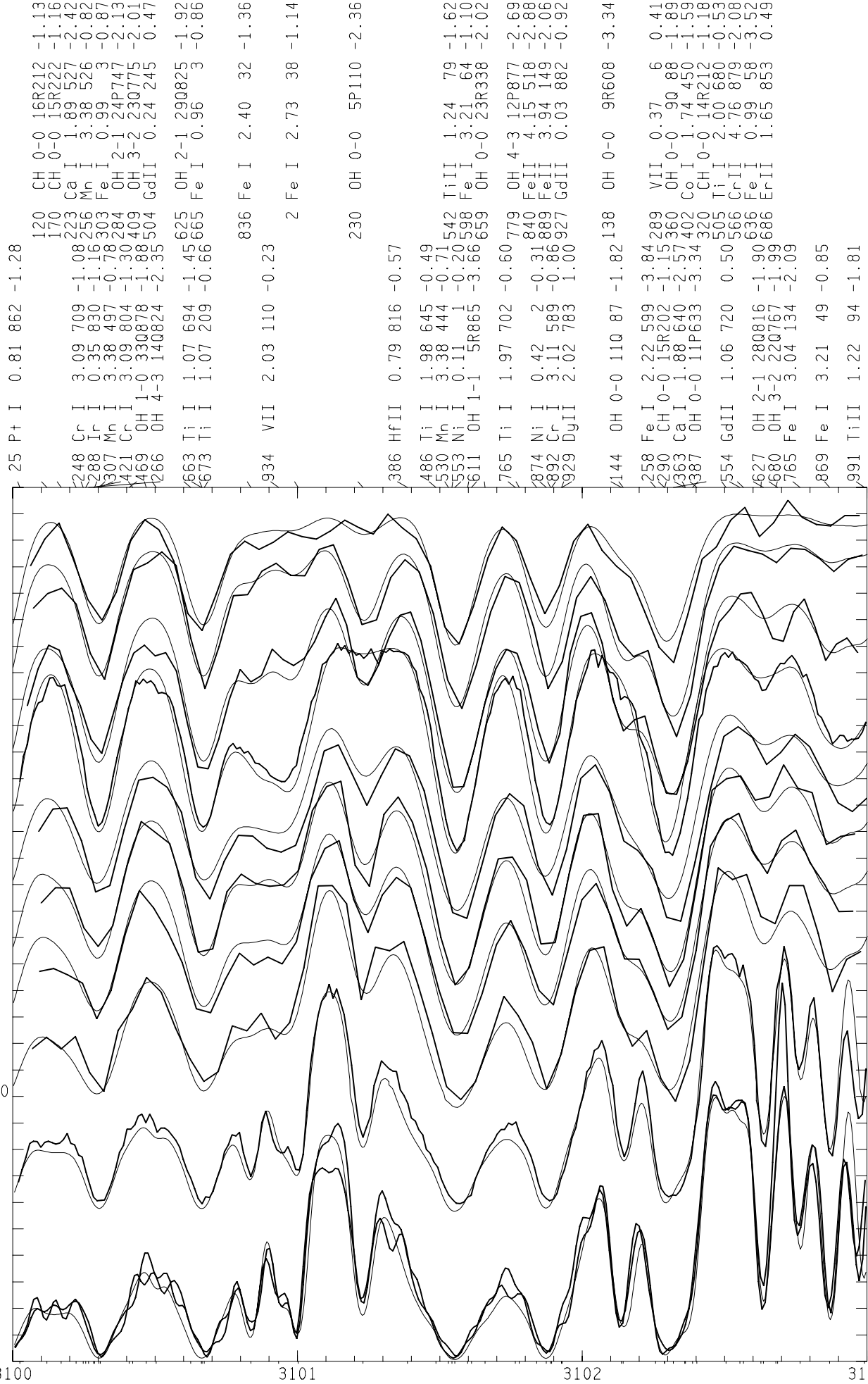
SCALE 1.10 5.26E+15 8.25E+17 1.54E+18 1.53E+18 9.18E+17 3.24E+17 3.60E+18 3.10E+18 4.78E+18



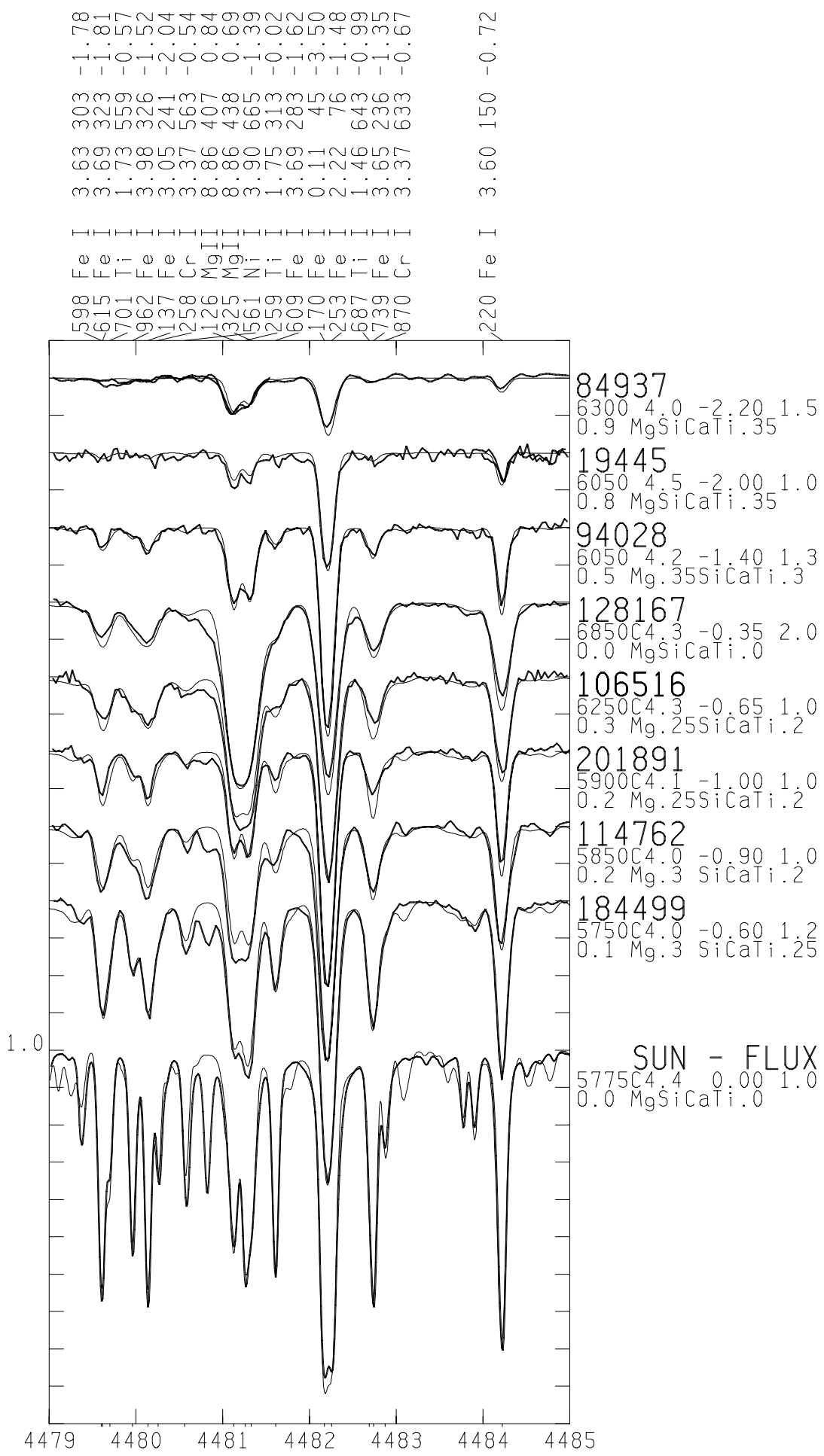
512	DvII	0.59	894	-0.69	524	VII	2.04	304	-0.97
605	OH 2-1	24P	696	-2.12	613	Co I	0.00	19	-1.34
642	Fe I	3.02	827	-3.55	613	Co I	0.00	19	-1.34
698	Mn I	4.23	654	-0.24	662	FeII	4.15	520	-2.88
846	Co I	1.88	212	-1.06					
921	Fe I	3.33	573	-2.72					
52	Fe I	3.40	742	-2.96	15	FeII	3.97	194	-2.32
147	Fe I	2.45	85	-2.26	65	Fe I	2.76	168	-2.56
212	VII	2.52	158	-0.08	190	Fe I	2.76	129	-2.36
278	OH 0-0	4P	286	-3.05	368	OH 4-3	120806	-2.41	
374	OH 0-0	4P	286	-3.05	368	OH 4-3	120806	-2.41	
488	Fe I	3.21	153	-2.04					
540	V I	1.22	638	-0.25					
601	CrII	4.07	279	-1.44					
665	CeII	0.79	618	0.35					
741	Fe I	0.99	3	-0.89					
831	OH 4-3	10P	871	-2.75					
890	OH 2-1	28Q	774	-1.90					
48	OH 0-0	0R	434	-3.31	70	Fe I	3.29	789	-3.18
141	OH 3-2	18P	694	-2.23					
300	Fe I	1.48	574	-4.52					
441	Cr I	2.71	622	-1.28	464	CeII	0.67	684	0.13
464	CrII	4.30	442	-1.56					
573	MnII	4.12	742	-1.95					
816	Ti I	1.05	642	-1.38					
896	OH 0-0	18R	180	-2.02					
40	Ti I	2.02	237	0.21	70	Fe I	3.41	900	-3.44
4197	OH 2-1	23P	702	-2.13	189	Cr I	3.08	647	-0.98
199	OH 0-0	50	89	-2.12					
292	Fe I	2.94	328	-2.74	279	CrII	4.07	869	-2.64
340	CrII	4.07	341	-1.58					
316	OH 0-0	5P	325	-3.10	400	Fe I	1.48	119	-3.62

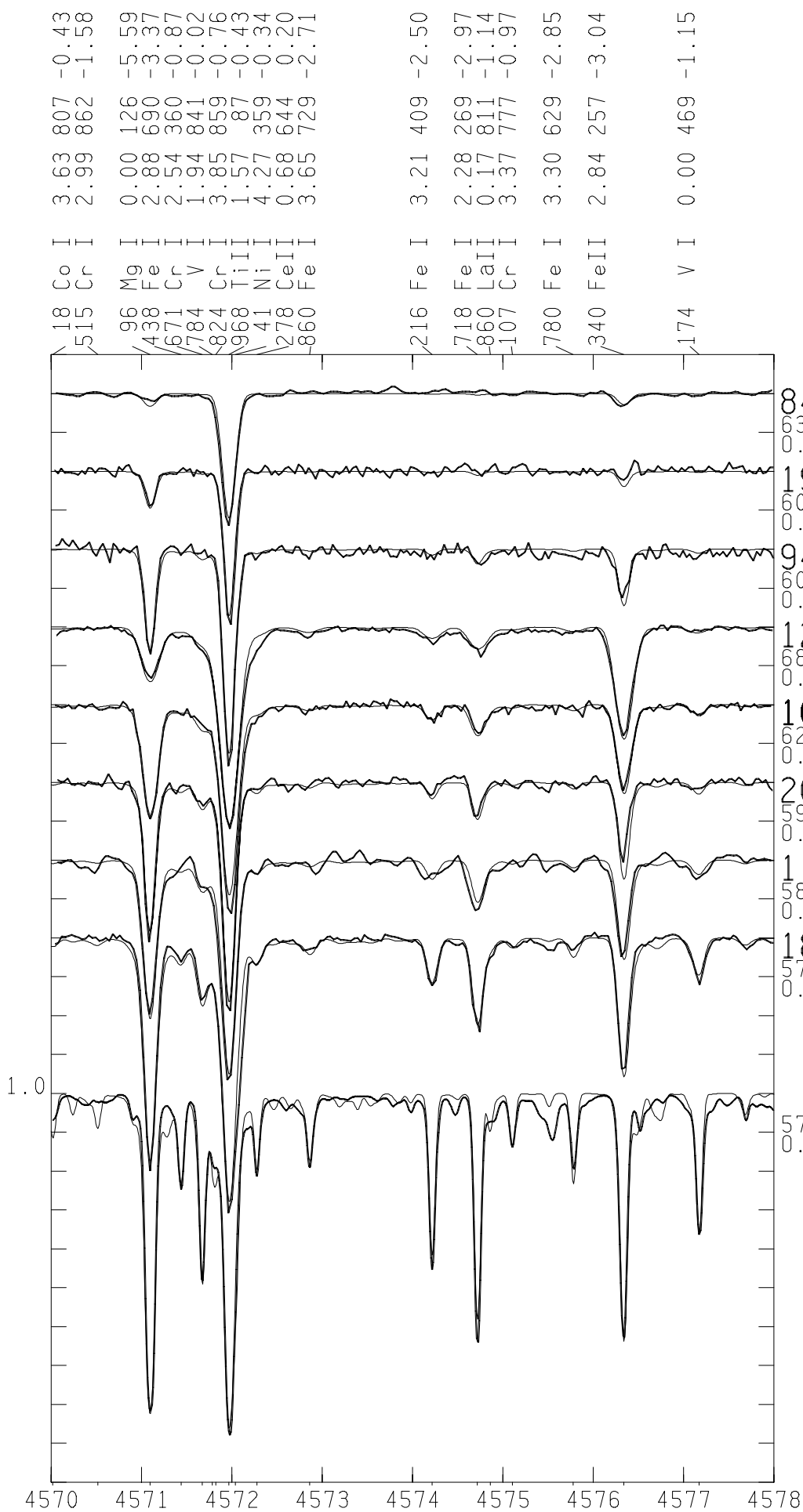
84937	6300	C4.0	-2.20	1.5
19445	6050	C4.5	-2.00	1.0
94028	6050	C4.2	-1.40	1.3
128167	6850	C4.3	-0.35	2.0
106516	6250	C4.3	-0.65	1.0
201891	5900	C4.1	-1.00	1.0
114762	5850	C4.0	-0.90	1.0
184499	5750	C4.0	-0.60	1.2
128620	5800	C4.3	0.15	1.0
SUN - CENTER	5775	C4.4	0.00	1.0

SCALE 1.10 5.26E+15 8.25E+17 1.54E+18 1.53E+18 9.18E+17 3.24E+17 3.60E+18 3.10E+18 4.78E+18



120	CH	0-0	16R212	-1.13
170	CH	0-0	15R222	-1.16
223	Ca	I	1.89 527	-2.42
248	Cr	I	3.38 526	-0.82
288	Ir	I	0.99 3	-0.87
307	Mn	I	2.24 747	-2.13
421	Cr	I	0H 3-2 230775	-2.01
469	OH	1-0	330878	-1.88 504
466	OH	4-3	140824	-2.35 245
663	Ti	I	1.07 694	-1.45 625
673	Ti	I	1.07 209	-0.66 665
836	Fe	I	2.40 32	-1.36
934	VII	2.03 110	-0.23	2 Fe I 2.73 38 -1.14
386	Hf	II	0.79 816	-0.57
486	Ti	I	1.98 645	-0.49
530	Mn	I	3.38 444	-0.71 542
553	Ni	I	0.11 1	-0.20 598
611	OH	1-1	5R865	-3.66 659
765	Ti	I	1.97 702	-0.60 779
874	Ni	I	0.42 2	-0.31 840
892	Cr	I	3.11 589	-0.86 927
929	Dy	II	2.02 783	1.00
1144	OH	0-0	110 87	-1.82 138
258	Fe	I	2.22 599	-3.84 289
290	CH	0-0	15R202	-1.15 360
363	Ca	I	1.88 640	-2.57 402
387	OH	0-0	11P633	-3.34 320
554	Gd	II	1.06 720	0.50 566
627	OH	2-1	280816	-1.90 636
680	OH	3-2	220767	-1.99 686
765	Fe	I	3.04 134	-2.09
869	Fe	I	3.21 49	-0.85
991	Ti	III	1.22 94	-1.81
84937	6300	C4.0	-2.20	1.5
19445	6050	C4.5	-2.00	1.0
94028	6050	C4.2	-1.40	1.3
128167	6850	C4.3	-0.35	2.0
106516	6250	C4.3	-0.65	1.0
201891	5900	C4.1	-1.00	1.0
114762	5850	C4.0	-0.90	1.0
184499	5750	C4.0	-0.60	1.2
128620	5800	C4.3	0.15	1.0
SUN - CENTER	5775	C4.4	0.00	1.0





84937
6300 C4.0 -2.20 1.5
0.9 MgSiCaTi.35

19445
6050 C4.5 -2.00 1.0
0.8 MgSiCaTi.35

94028
6050 C4.2 -1.40 1.3
0.5 Mg.35SiCaTi.3

128167
6850 C4.3 -0.35 2.0
0.0 MgSiCaTi.0

106516
6250 C4.3 -0.65 1.0
0.3 Mg.25SiCaTi.2

201891
5900 C4.1 -1.00 1.0
0.2 Mg.25SiCaTi.2

114762
5850 C4.0 -0.90 1.0
0.2 Mg.3 SiCaTi.2

184499
5750 C4.0 -0.60 1.2
0.1 Mg.3 SiCaTi.25

SUN - FLUX
5775 C4.4 0.00 1.0
0.0 MgSiCaTi.0

